Magnetic anisotropy in metallic multilayers

Rep. Prog. Phys. **59** (1996) 1409–1458. Printed in the UK

Magnetic anisotropy in metallic multilayers

M T Johnson†, P J H Bloemen‡§, F J A den Broeder† and J J de Vries‡

† Philips Research Laboratories, Prof. Holstlaan 4, 5656 AA Eindhoven, The Netherlands
‡ Eindhoven University of Technology, Department of Physics, PO Box 513, 5600 MB Eindhoven, The Netherlands

Received 25 July 1996

Abstract

Ferromagnetic materials exhibit intrinsic 'easy' and 'hard' directions of the magnetization. This magnetic anisotropy is, from both a technological and fundamental viewpoint one of the most important properties of magnetic materials. The magnetic anisotropy in metallic magnetic multilayers forms the subject of this review article. As individual layers in a multilayer stack become thinner, the role of interfaces and surfaces may dominate that of the bulk: this is the case in many magnetic multilayers, where a perpendicular interface contribution to the magnetic anisotropy is capable of rotating the easy magnetization direction from in the film plane to perpendicular to the film plane. In this review, we show that the (in-plane) volume and (perpendicular) interface contribution to the magnetic anisotropy have been separated into terms related to mechanical stresses, crystallographic structure and the planar shape of the films. In addition, the effect of roughness, often inherent to the deposition techniques used, has been addressed theoretically. Several techniques to prepare multilayers and to characterize their growth as well as methods to determine the magnetic anisotropy are discussed. A comprehensive survey of experimental studies on the perpendicular magnetic anisotropy in metallic multilayers containing Fe, Co or Ni is presented and commented on. Two major subjects of this review are the extrinsic effects of strain, roughness and interdiffusion and the intrinsic effect of the crystallographic orientation on the magnetic anisotropy. Both effects are investigated with the help of some dedicated experimental studies. The results of the orientational dependence studies are compared with *ab initio* calculations. Finally, the perpendicular surface anisotropy and the in-plane step anisotropy are discussed.

§ Present address: Philips Research Laboratories, Prof. Holstlaan 4, 5656 AA Eindhoven, The Netherlands

0034-4885/96/111409+50$59.50

Contents

1. Introduction

It is an experimental fact that ferromagnetic single crystals exhibit 'easy' and 'hard' directions of the magnetization; i.e. the energy required to magnetize a crystal depends on the direction of the applied field relative to the crystal axes. From the technological viewpoint this *magnetic anisotropy* is one of the most important properties of magnetic materials. Depending on the type of application, material with high, medium or low magnetic anisotropy will be required, for respective application as, for example, permanent magnets, information storage media or magnetic cores in transformers and magnetic recording heads.

The physical basis that underlies a preferred magnetic moment orientation in ultrathin magnetic films and multilayers can be quite different from the factors that account for the easy-axis alignment along a symmetry direction of a bulk material, and the strength can also be markedly different. The prominent presence of symmetry-breaking elements such as planar interfaces and surfaces, which automatically accompany the layered form of these systems, are the basic ingredients for this behaviour. By varying the thicknesses of the individual layers and choosing appropriate materials, it appeared possible to tailor the magnetic anisotropy. The most dramatic manifestation in this respect is the change of the preferential direction of the magnetization from the commonly observed in-plane orientation to the direction perpendicular to the plane. This phenomenon is usually referred to as perpendicular magnetic anisotropy (PMA) and is particularly important for information storage and retrieval applications.

PMA plays an important role in magneto-optical (MO) recording. To write bits in MO media, the disk is heated locally by a pulse of a diode laser beam which is focused to a spot of about 1 μm (see also figure 1). The magnetization is reversed only in the area of the heated spot by applying a small bias counter field, which is smaller than the coercive field of

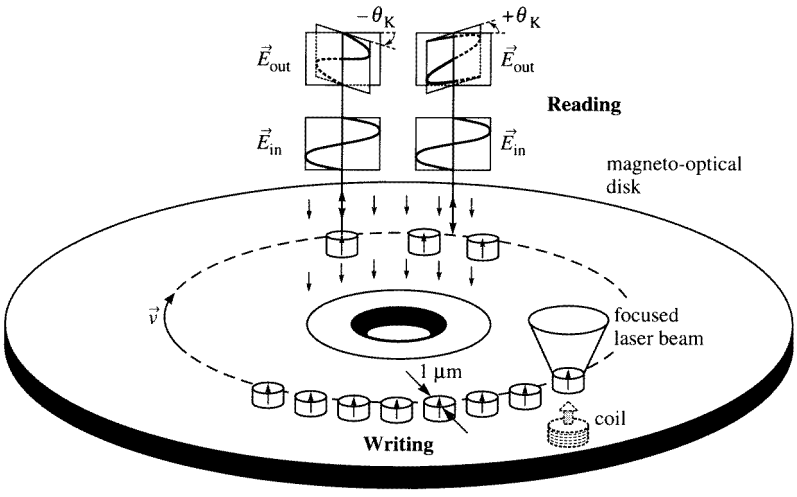

Figure 1. Schematic representation of the principle of magneto-optical recording (Zeper 1991). For more information see text.

the MO layer at room temperature but larger than the coercive field in the heated area. The same laser that is used for writing also reads back the written bits (domain pattern) making use of the polar magneto-optical Kerr effect, the effect that the polarization of the light is changed (i.e. rotation of the plane of linear polarization over an angle θ_K) upon reflection at a magnetic surface (Kerr 1877). Since the latter is most sensitive to the perpendicular component of the magnetization, one of the principle requirements of an MO medium is a perpendicular preferential orientation. Today's MO materials, the amorphous Gd–Tb–Fe and Tb–Fe–Co alloys, meet this requirement and have a sufficient Kerr effect. However, apart from intrinsic deficiencies such as their susceptibility to corrosion and oxidation, their Kerr effect considerably decreases at shorter wavelengths λ of the light. They therefore oppose a further increase in the storage density since the latter is largely determined by the diffraction limited spot area being proportional to λ^2. Several metallic magnetic multilayers appeared *not* to exhibit these disadvantages. This application possibility of magnetic multilayers with PMA formed one of the principle motivations for many groups to enter the field and is still in part responsible for the current world-wide attention for these systems. In addition, new phenomena such as the interlayer exchange coupling and the giant magnetoresistance have also attracted considerable attention in the last decade, see Fert and Bruno (1994) for a recent review on the latter two topics.

The PMA is a result of a magnetic anisotropy at the interface which considerably differs from the magnetic anisotropy in the bulk. This type of magnetic anisotropy, a so-called interface or surface anisotropy, was predicted already in 1954 by Néel (1954) to result from the lowered symmetry at the surface or interface. The first experiments which had revealed such an interface anisotropy were performed in 1968 by Gradmann and Müller (1968) on ultrathin NiFe films on Cu(111). What they observed was an easy axis perpendicular to the film plane for 1.8 monolayers of NiFe and furthermore that the magnetic anisotropy scaled with the reciprocal film thickness. For multilayers PMA was first observed in 1985 by Carcia *et al* in the Co/Pd system Carcia *et al* (1985) and later on in several other Co-based multilayers: Co/Pt (Carcia 1988), Co/Au (den Broeder *et al* 1988), Co/Ru (Sakurai *et al* 1991) and Co/Ir (den Broeder *et al* 1991).

In these studies the (effective) magnetic anisotropy energy K (J m^{-3}) could be phenomenologically separated in a volume contribution K_v (J m^{-3}) and a contribution from the interfaces K_s (J m^{-2}) and approximately obeyed the relation:

$$K = K_{\mathrm{eff}} = K_v + 2K_s/t. \tag{1}$$

This relation just represents a weighted average of the magnetic anisotropy energy (MAE) of the interface atoms and the inner atoms of a magnetic layer of thickness t. The relation is presented under the convention that K_s/d (with d the thickness of a monolayer) represents the difference between the anisotropy of the interface atoms with respect to the inner or bulk atoms. Also the layer is assumed to be bounded by two identical interfaces accounting for the prefactor 2. Equation (1) is commonly used in experimental studies, and the determination of K_v and K_s can be obtained by a plot of the product $K_{\mathrm{eff}}t$ versus t. Figure 2 shows a typical example of such a plot for Co/Pd multilayers (den Broeder *et al* 1991). Here, and in the following, a positive K_{eff} describes the case of a preferred direction of the magnetization perpendicular to the layer plane. The negative slope indicates a negative volume anisotropy K_v, favouring in-plane magnetization, while the intercept at zero Co thickness indicates a positive interface anisotropy K_s, favouring perpendicular magnetization. Below a certain thickness $t_\perp$ ($= -2K_s/K_v$, in this case 13 Å) the interface anisotropy contribution outweighs the volume contribution, resulting in a perpendicularly magnetized system. In other words, the strong demagnetizing fields which are created when tilting the magnetization out of

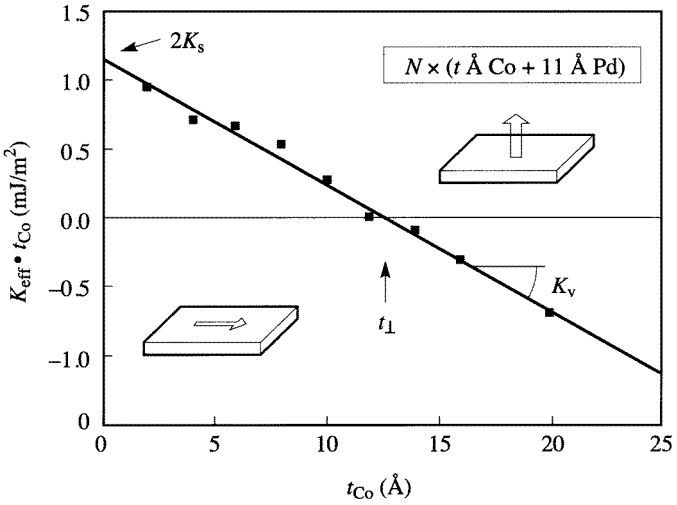

Figure 2. MAE times the individual Co layer thickness versus the individual Co layer thickness of Co/Pd multilayers. The vertical axis intercept equals twice the interface anisotropy, whereas the slope gives the volume contribution. Data are taken from den Broeder *et al* (1991).

the film plane and which are usually responsible for the orientation of the magnetization parallel to the film plane, are overcome. As will be shown later on, the volume energy corresponding to these demagnetizing fields form the major contribution to K_v in most cases.

The many experimental results of the type shown in figure 2 considerably stimulated theoretical work. For the bulk transition metals, it appeared very difficult to calculate the magnetic anisotropy from first principles. The order of magnitude was correct, but the predicted sign was often wrong (Daalderop *et al* 1990a). These difficulties are related to the fact that the corresponding energies are very small (of the order of 1 meV per atom). However, for multilayers and ultrathin films, which exhibit generally larger anisotropies, much progress has recently been made. For several Co based multilayers, good agreement has been reached between first principles calculated anisotropies and the corresponding experimental values (Daalderop *et al* 1990b). To increase the general understanding, these calculations can now, in principle, be used to calculate the magnetic anisotropy of magnetic layers and multilayers which cannot be made under laboratory conditions, such as free-standing monolayers; alternatively, one can make predictions for multilayers that have not been studied experimentally previously. An example of the latter is formed by Co/Ni multilayers (Daalderop *et al* 1992).

This review article is primarily concerned with the *experimental* aspects of the research performed on the magnetic anisotropy in thin films and multilayers. A restriction has been made to (multi)layers containing transition metals; rare-earth transition metal multilayers are not considered. Moreover, the (perpendicular) uniaxial out-of-plane anisotropy is emphasized although in-plane anisotropies will also be addressed. Earlier reviews on magnetic anisotropy were given by Heinrich and Cochran (1993) and de Jonge *et al* (1994).

The article is organized as follows. Section 2 deals with the theory of several contributions to the magnetic anisotropy of magnetic thin films. The most commonly used experimental techniques to quantitatively determine the magnetic anisotropy are briefly introduced in section 3. In section 4, a compilation of the currently used techniques to

grow, as well as to characterize films and multilayers, is given and the advantages and disadvantages are mentioned. An extensive overview of the measured magnetic anisotropies is given in section 5. Section 6 is devoted to several aspects of the growth conditions and film structure which influence the PMA in magnetic multilayers, such as roughness and interdiffusion, stress and preparation methods. The orientational dependence of the magnetic anisotropy is discussed in relation with theoretical calculations in section 7. The remaining sections deal with the magnetic anisotropy generated at free surfaces, section 8, and surface steps, section 9. In view of the limited space a selection of interesting studies has been made so as to cover, as much as possible, different aspects that are of importance for the general understanding of the magnetic anisotropy of ultrathin magnetic layers. The authors apologise to those whose work is not explicitly mentioned. The field has become too large to cover all interesting studies in one paper.

Included are tables of multilayers and sandwiches exhibiting PMA studied so far and of the orientational dependence of the PMA in Co/Pt, Co/Pd and Co/Ni multilayers. Other topics are a study on the Cu/Ni system emphasizing the importance of magneto-elastic contributions for both interface and volume anisotropy terms and a systematic experimental investigation of the relation between the magnetic anisotropy and the interface roughness.

2. Origin of the magnetic anisotropy in thin films

Basically, the two main sources of the magnetic anisotropy are the magnetic dipolar interaction and the spin–orbit interaction. Due to its long range character, the dipolar interaction generally results in a contribution to the anisotropy, which depends on the shape of the specimen. It is of particular importance in thin films, and is largely responsible for the in-plane magnetization usually observed. In the absence of spin–orbit and dipolar interaction, the total energy of the electron–spin system does not depend on the direction of the magnetization. In a localized picture the spins are coupled via the spin–orbit interaction to the orbits which, in turn, are influenced by the crystal lattice. For itinerant materials the spin–orbit interaction induces a small orbital momentum, which then couples the total (spin plus orbital) magnetic moment to the crystal axes. This results in a total energy which depends on the orientation of the magnetization relative to the crystalline axes, and which reflects the symmetry of the crystal. This is known as the magnetocrystalline contribution to the anisotropy. The lowered symmetry at an interface strongly modifies this contribution as compared to the bulk, yielding, as mentioned already, a so-called interface anisotropy as pointed out by Néel (1954). In conjunction with the overlap in wavefunctions between neighbouring atoms, the spin–orbit interaction is also responsible for the magneto-elastic or magnetostrictive anisotropy induced in a strained system, a situation which is frequently encountered in multilayers due to the lattice mismatch between the adjacent layers. In the following subsections each of these anisotropy terms will be discussed in somewhat more detail.

2.1. Magnetic dipolar anisotropy (shape anisotropy)

Among the most important sources of the magnetic anisotropy in thin films is the long range magnetic dipolar interaction, which senses the outer boundaries of the sample. Neglecting the discrete nature of matter, the shape effect of the dipolar interaction in ellipsoidal ferromagnetic samples can be described, via an anisotropic demagnetizing field, $\boldsymbol{H}_{\mathrm{d}}$, given by $\boldsymbol{H}_{\mathrm{d}} = -\mathcal{N}\boldsymbol{M}$. Here $\boldsymbol{M}$ is the magnetization vector and $\mathcal{N}$ is the shape-dependent demagnetizing tensor. For a thin film, all tensor elements are zero except for the direction

perpendicular to the layer: $\mathcal{N}^{\perp} = 1$. Since the magnetostatic energy can be expressed as

$$E_{\mathrm{d}} = -\frac{\mu_0}{2V}\int \boldsymbol{M}\cdot\boldsymbol{H}_{\mathrm{d}}\,\mathrm{d}v \tag{2}$$

where μ_0 is the permeability of vacuum, it results in an anisotropy energy contribution per unit volume V of a film of:

$$E_{\mathrm{d}} = \tfrac{1}{2}\mu_0 M_{\mathrm{s}}^2\cos^2\theta. \tag{3}$$

Here the magnetization is assumed to be uniform with a magnitude equal to the saturation magnetization M_{s}, and subtends an angle θ with the film normal. According to this expression, the contribution favours an in-plane preferential orientation for the magnetization. Because the thickness of the film does not enter into the continuum approach employed above, it contributes only to K_{v}. It is this contribution which is mainly responsible for the negative slope of the $K_{\mathrm{eff}}t$ versus t plot in figure 2. This continuum approach is common in the analysis of the experimental data.

However, when the thickness of the ferromagnetic layer is reduced to only a few monolayers (ML), the film should not, in principle, be considered as a magnetic continuum, but has to be treated as a collection of discrete magnetic dipoles on a regular lattice. Calculations made on the basis of discretely summing the dipolar interactions for films in the range of 1–10 MLs lead to the following results (Draaisma and de Jonge 1988). Depending on the symmetry of the interface, the outer layers experience a dipolar anisotropy which can be appreciably lower than the inner layers. For the inner layers, the dipolar anisotropy is rather close to the value based on the continuum approach. Consequently, the average dipolar anisotropy can be phenomenologically expressed by a volume and an interface contribution. The magnitude of the dipolar interface contribution, however, is of minor importance, and other sources of interface anisotropy, such as spin–orbit coupling, appear to be dominant.

2.2. Magnetocrystalline anisotropy

As stated before, the microscopic origin of the magnetocrystalline anisotropy is the spin–orbit interaction. In principle, also the exchange interaction and the dipolar interaction could contribute to the magnetocrystalline anisotropy. The exchange interaction, however, cannot give rise to anisotropy since it is proportional to the scalar product of the spin vectors and is therefore independent of the angle between the spins and the crystal axes. The dipolar interaction energy on the other hand, does depend on the orientation of the magnetization relative to the crystal axes. In principle it results, apart from the shape contribution already discussed in subsection 2.1, in a magnetocrystalline contribution. However, for cubic crystals it can be shown from symmetry arguments that the sum of the dipole–dipole energies cancels. For structures with lower symmetry, such as hexagonal crystals, this is generally not the case. For bulk hcp cobalt however, this contribution is negligible, since the deviation of the c/a ratio from the ideal value $\sqrt{8/3}$ is relatively small (-0.67%) (Daalderop *et al* 1990a). Consequently, the spin–orbit interaction will be primarily responsible for the magnetocrystalline anisotropy in Fe, Ni (both cubic) and Co.

Before a good understanding of itinerant electron behaviour was achieved, van Vleck discussed the magnetocrystalline anisotropy (in the case of bulk) in a pair interaction model assuming localized magnetic moments (van Vleck 1937). Néel (1954) extended this model to surfaces and showed that the reduced symmetry at the surface should result in magnetic anisotropies at the surface differing strongly from the bulk atoms. For this surface anisotropy energy he derives for fcc(111) and fcc(100) surfaces for instance, the

relation $E = -K_s \cos^2\theta$, with K_s differing for (111) and (100) surfaces. Although the pair interaction model also played a role in the discussion about roughness and interdiffusion, as discussed later, and contributed significantly to the understanding, it is fundamentally incorrect. It does not discriminate between interface and surface, nor does it give a dependence of K_s on the adjacent (non-magnetic) metal. In some cases it predicts the wrong sign. Throughout this text, in fact, interface anisotropy will be considered except in section 8 where the surface anisotropy is discussed.

A thorough understanding of the magnetocrystalline anisotropy can now be obtained from *ab initio* bandstructure calculations. As shown in (Daalderop 1991), the symmetry and location with respect to the Fermi level of spin–orbit split or shifted states are of major importance. The symmetry of the state for instance, determines whether or not the state is split if the direction of the magnetization is perpendicular or parallel to the film plane, i.e. it determines the sign of the contribution of the state to the magnetocrystalline anisotropy. For further and more detailed discussions the reader is referred to (Daalderop *et al* 1994). A short summary of the current status of the theory is presented in subsection 7.4.

2.3. Magneto-elastic anisotropy

Strain in a ferromagnet changes the magnetocrystalline anisotropy and may thereby alter the direction of the magnetization. This effect is the 'inverse' of magnetostriction, the phenomenon that the sample dimensions change if the direction of the magnetization is altered. The energy per unit volume associated with this effect can, for an elastically isotropic medium with isotropic magnetostriction, be written as

$$E_{me} = -K_{me}\cos^2\theta \tag{4}$$

with

$$K_{me} = -\tfrac{3}{2}\lambda\sigma \tag{5}$$

$$= -\tfrac{3}{2}\lambda E\epsilon. \tag{6}$$

Here σ is the stress which is related to the strain, ϵ, via the elastic modulus E by $\sigma = E\epsilon$. The magnetostriction constant λ depends on the orientation and can be positive or negative. The angle θ measures the direction of the magnetization relative to the direction of uniform stress. If the strain in the film is non-zero, the magneto-elastic coupling contributes in principle to the effective anisotropy. When the parameters are constant (not depending on the magnetic layer thickness, t) this contribution can be identified with a volume contribution K_v (compare equation (1)).

Strain in films can be induced by various sources. Among them are thermal strain associated with differences in thermal expansion coefficients, intrinsic strain brought about by the nature of the deposition process and strain due to non-matching lattice parameters of adjacent layers.

Of particular interest in the present context, is the strain due to lattice mismatch η of a material A deposited on material B:

$$\eta = (a_A - a_B)/a_A \tag{7}$$

where a is the lattice parameter of material A or B. Currently this problem is described in terms of the van der Merwe model in which elastic as well as dislocation energies are considered (van der Merwe 1963). Two regimes should be distinguished. If the lattice mismatch between the lattice parameters is not too large, minimizing the total energy leads to a situation whereby, below a critical thickness t_c, the misfit can be accommodated by

introducing a tensile strain in one layer and a compressive strain in the other such that ultimately the two materials A and B adopt the same in-plane lattice parameter. This regime is called the *coherent* regime, the lateral planes are in full lattice-registry.

The strain as well as t_c depend strongly on the specific geometry (bilayer, sandwich, film on a substrate, multilayer, etc). For a general multilayer A/B in the coherent regime, minimization of the elastic energy ($\frac{1}{2}tE\epsilon^2$), yields in good approximation:

$$\epsilon_A = -\eta/(1 + t_A E_A/t_B E_B) \tag{8}$$

$$\epsilon_B = \eta + \epsilon_A \tag{9}$$

with E_A and E_B the elastic moduli of layer A and B. For other geometries, analogous relations can be derived. Assuming that layer A is the magnetic layer, substitution of ϵ_A in equation (6) gives the magneto-elastic contribution to the anisotropy $K_{me}^{coh} = -\frac{3}{2}\lambda E_A \epsilon_A$. In principle, this contribution contains the thickness of the magnetic layer t_A, and therefore may obscure the simple analysis in terms of volume and interface contributions (equation (1)). In the specific cases of $t_A \ll t_B$ and $t_A/t_B =$ constant, the magneto-elastic anisotropy is independent of t_A and contributes only to K_v:

$$K_{me,v}^{coh} = \tfrac{3}{2}\lambda E_A \eta. \tag{10}$$

The elastic energy associated with the coherent situation is proportional to the strained volume. Increasing the thickness of layer A will therefore increase the elastic energy. This energy increase will not persist. At a certain critical thickness t_c, already mentioned above, it becomes energetically more favourable to introduce misfit dislocations which partially accommodate the lattice misfit, allowing the uniform strain to be reduced. The lattice-registry is then partially lost and the layers become partially coherent or in short *incoherent*.

In general, it is not an easy task to calculate the strain in the incoherent regime. In the special case of a single layer A on a rigid substrate it has been shown (Matthews 1990, Chappert and Bruno 1988), by minimization of the sum of the elastic energy and the energy due to dislocations, that the residual strain ϵ_A, which is assumed to be uniform within the layer, can be written as

$$\epsilon_A = -\eta t_c/t_A \tag{11}$$

where t_c, in first approximation, is given by (den Broeder *et al* 1991):

$$t_c = \frac{Gb}{8|\eta|E_A}. \tag{12}$$

Here use was made of the simple expression for the energy of a dislocation $E = \frac{1}{2}Gb^2$, where b is the Burgers vector of the dislocation and G the shear modulus. The critical thickness t_c in the case of a thin layer A sandwiched between two identical layers B is four times larger since two layers B are elastically deformed, while there are two interfaces A/B to mediate the stress (den Broeder *et al* 1991). Alternatively, by considering the strain field around a misfit dislocation, Matthews and Blakeslee (1974, 1975) derived a critical thickness:

$$\frac{t_c}{b} = \frac{Gx}{4\pi|\eta|E_A}\ln\left(\frac{t_c}{b} + 1\right) \tag{13}$$

where $x = 1$ for a single layer deposited on a substrate and $x = 2$ if the stressed layer is sandwiched between two considerably thicker layers which both support coherent growth. This expression has been used for comparison with the experiment in subsection 6.2. As a consequence of the specific form of equation (11), the contribution of the magneto-elastic energy, equation (6), also contains the $1/t$ dependence. Following the common analysis

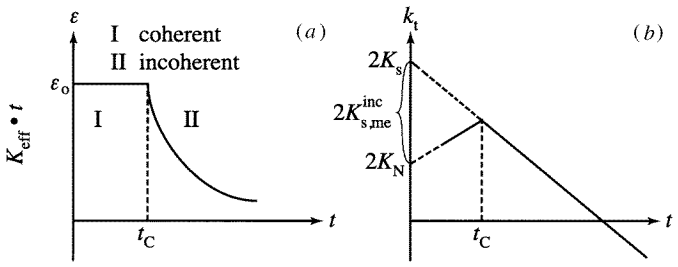

Figure 3. Theoretical thickness dependence of (*a*) the strain and (*b*) the MAE times the layer thickness in the coherent and incoherent regime.

of anisotropy data as introduced by equation (1), this contribution, which is essentially generated in the volume, will emerge as an apparent interface contribution for the incoherent growth regime:

$$K_{me} = \tfrac{3}{2}\lambda E_A \eta t_c / t_A. \tag{14}$$

By substituting $K_{me} = 2K_{me,s}^{inc}/t_A$, the interface anisotropy is found to be:

$$K_{me,s}^{inc} = \tfrac{3}{4}\lambda E_A \eta t_c. \tag{15}$$

It should be noted that $K_{me,s}^{inc}$ does not depend on η because its dependence cancels against that of t_c, see equations (12) and (13). An alternative, simple expression for the magneto-elastic interface contribution in the case of a sandwiched layer, can be given in terms of G and b (den Broeder *et al* 1991) ($\eta < 0$):

$$K_{me,s}^{inc} = -\tfrac{3}{8}\lambda G b. \tag{16}$$

Figure 3 illustrates the transition between the coherent and incoherent regime and the resulting effect observed in the magnetic anisotropy. Thus, a separate interpretation of the magnetic anisotropy must be made in the regions above and below t_c (den Broeder *et al* 1991). In the coherent region below t_c, the volume anisotropy K_v incorporates shape anisotropy, magnetocrystalline anisotropy (K_{mc}) and strain anisotropy ($K_{me,v}$), with interface anisotropy being solely Néel-type.

$$K_s = K_N \tag{17}$$

$$K_v = -\tfrac{1}{2}\mu_o M_s^2 + K_{mc} + K_{me,v}^{coh} \tag{18}$$

with $K_{me,v}^{coh}$ as in equation (10). In this region, the influence of misfit strain thus appears as a volume contribution to the anisotropy. In the incoherent region above t_c, the distinctive form of volume strain represented by equation (11) has been shown to lead to an apparent interface contribution: the magneto-elastic interface anisotropy (Chappert and Bruno 1988), so that:

$$K_s = K_N + K_{me,s}^{inc} \tag{19}$$

$$K_v = -\tfrac{1}{2}\mu_o M_s^2 + K_{mc} \tag{20}$$

with $K_{me,s}^{inc}$ as in equation (15). Figure 3(*b*) schematically illustrates the expected dependence of $K_{eff}t$ on t, with a marked kink appearing at the critical thickness t_c. The relevance of this picture will be discussed by considering the Cu/Ni model system, in subsection 6.2.

3. Techniques to determine magnetic anisotropy

Magnetic anisotropy can be deduced from the dynamical response of the magnetic system or from the static response. The dynamic response of the magnetic layers can be measured by ferromagnetic resonance (FMR) and Brillouin light scattering (BLS). For a review on these techniques the reader is referred to (Heinrich 1994, Cochran 1994, Hillebrands and Güntherodt 1994). The static response can be measured by torque magnetometry, torsion oscillating magnetometry (TOM) (Bergholz and Gradmann 1984), the magneto-optical Kerr effect (MOKE) (Purcell *et al* 1992) and various techniques which measure the magnetic moment, such as vibrating sample magnetometry (VSM) (Zijlstra 1967), superconducting quantum interference device (SQUID) magnetometry, fluxgate magnetometry, alternating gradient magnetometry (AGM) (Flanders 1988), pendulum magnetometry, Faraday balance, etc.

Much of the experimental data so far has been obtained from static measurements. In particular magnetization and torque measurements are frequently employed to determine the magnetic anisotropy. This section is restricted to an introduction of the magnetization experiments. For a discussion on the analysis of torque measurements see Burd *et al* (1977), Swaving *et al* (1987) and Artman (1985). Furthermore, the use of the Kerr effect as a local probe in anisotropy studies will be introduced.

3.1. Magnetization methods

The magnetic anisotropy is most frequently determined from magnetization measurements, e.g. by VSM or SQUID, along two orthogonal directions of the magnetic field relative to the sample. Examples of such measurements, with the field parallel and perpendicular to the film plane, are shown in figure 4. Here the upper two graphs correspond to samples where the preferential direction is clearly perpendicular. The MAE is given by the area enclosed between the parallel and perpendicular loops. This is based on elementary electromagnetic considerations which show that the energy needed to change the sample magnetization in an applied field H by an amount $\mathrm{d}M$ is given by $\mu_0 H\,\mathrm{d}M$. In some cases, as demonstrated later, the MAE can also be obtained from the fields at which saturation occurs.

The angle-dependent part of the energy E of the magnetization of the thin film can be written as

$$E = (-K_\mathrm{i} + \tfrac{1}{2}\mu_0 M_\mathrm{s}^2)\cos^2\theta - \mu_0 M_\mathrm{s} H\cos(\phi - \theta). \tag{21}$$

In this expression, K_i contains all first-order (intrinsic) anisotropy energy contributions except the shape anisotropy or magnetostatic energy contribution, which is given by $\frac{1}{2}\mu_0 M_\mathrm{s}^2$ for a saturated film (compare equation (3)). The last term describes the interaction between the applied field and the resulting magnetization; θ and ϕ denote the angles subtended by the magnetization and field, respectively, and the film normal. Energy minimization as a function of the applied field H yields the field dependence of the equilibrium angle $\theta_\mathrm{eq}(H)$ and the field component of the magnetization $M = M_\mathrm{s}\cos(\theta_\mathrm{eq} - \phi)$.

For samples with an in-plane easy axis ($K_\mathrm{eff} = K_\mathrm{i} - \frac{1}{2}\mu_0 M_\mathrm{s}^2 < 0$) this procedure gives the magnetization curves shown in figure 5(*a*). The area enclosed between the two curves clearly equals the effective MAE, K_eff. As the figure shows, the MAE could in this case also be obtained from the hard-axis saturation field, the so-called anisotropy field $H_\mathrm{A} = -2K_\mathrm{eff}/\mu_0 M_\mathrm{s}$.

In the case of samples with a perpendicular easy axis ($K_\mathrm{eff} > 0$) one should be careful in applying this analysis. Consider as a starting point ($H = 0$) a situation in which the film

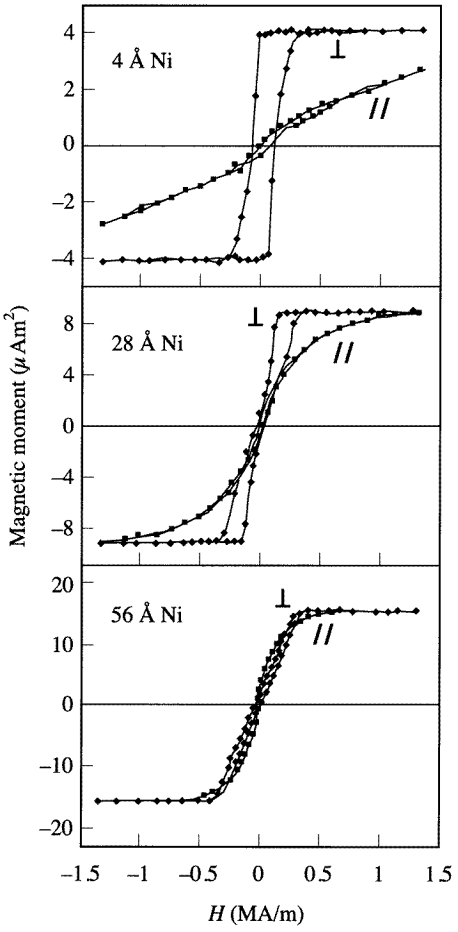

Figure 4. Hysteresis loops measured with the applied field parallel and perpendicular to the layer plane of a $30\times$(2 Å Co+$t_{\rm Ni}$Ni+2 Å Co+10 Å Pt) multilayer for $t_{\rm Ni}$ = 4, 28, 56 Å, after Bloemen and de Jonge (1992).

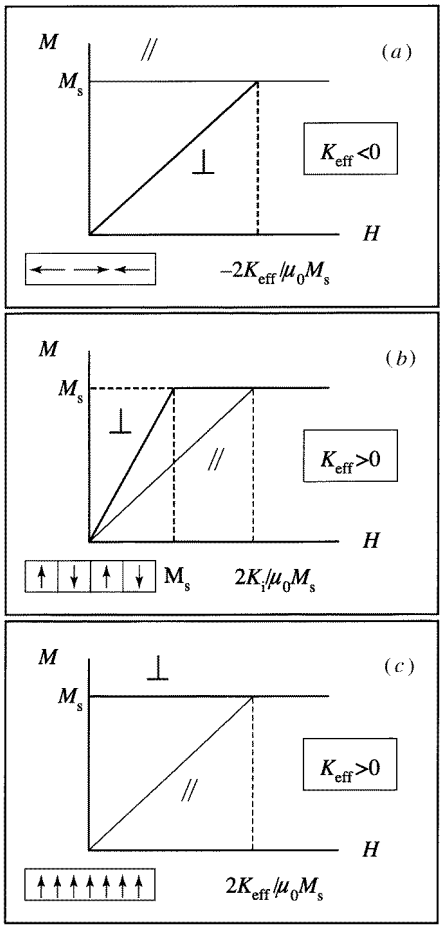

Figure 5. Magnetization curves for magnetic layers having an in-plane (*a*) or perpendicular (*b*, *c*) preferential orientation; (*b*) situation with small domains; (*c*) situation with large domains. Fields are applied along the parallel (∥) or perpendicular (⊥) direction.

consists of alternately up and down oriented domains of equal size, as shown schematically near the origin of figure 5(*b*). The magnetostatic energy contribution used in equation (21) is then not valid in general because it depends on the size of the domains (Kooy and Enz 1960).

For very small domains, the magnetostatic interaction between the domains is such that the magnetostatic term can be described by: $\frac{1}{2}\mu_0 M_\perp^2$, with $M_\perp$ the average perpendicular component of the magnetization. The perpendicular magnetization curve can then be obtained by minimizing $E = \frac{1}{2}\mu_0 M_\perp^2 - \mu_0 M_\perp H$ with respect to the magnetization. Here the $-K_{\rm i}\cos^2\theta$ term being constant (the magnetization either points up ($\theta = 0$) or down ($\theta = \pi$) in perpendicular applied fields, with $K_{\rm eff} > 0$) is omitted. Setting $\partial E/\partial M_\perp = 0$ yields $M_\perp = H$ giving rise to a non-zero saturation field. For in-plane applied fields, $\frac{1}{2}\mu_0 M_\perp^2$ is always zero and the magnetization curve is obtained by minimization of

$-K_i \cos^2\theta - \mu_0 M_s H \cos(\frac{1}{2}\pi - \theta)$ with respect to θ. The resulting curves are shown in figure 5(*b*). In this case the saturation fields have no direct relation to K_{eff}. Nevertheless, the area between the curves still represents the effective MAE, K_{eff}, including the shape anisotropy.

In the case of very large domains, the effect of the interaction between the domains is negligible and, although at $H = 0$ the average perpendicular component of the magnetization is zero, the magnetostatic energy term is correctly described as in equation (21) for both perpendicular and in-plane applied fields. When magnetizing the layer perpendicularly, the magnetostatic energy does not have to be overcome. Minimization of equation (21) therefore gives a perpendicular curve saturating immediately and an in-plane curve saturating at the field $2K_i/\mu_0 M_s - M_s$ or $2K_{eff}/\mu_0 M_s$, see figure 5(*c*). As in the previous cases, the area between the in-plane and perpendicular magnetization curve gives the effective MAE, K_{eff}, including the shape anisotropy energy.

The general case of arbitrary domain size has been treated by Kooy and Enz (1960). Their analysis shows that the dimensionless parameter $\tau = \frac{1}{2}\mu_0 M_s^2 4t/\pi\gamma$, with γ the domain wall energy per unit area and t the thickness of the magnetic layer, largely determines the domain size. The magnetostatic energy $\frac{1}{2}\mu_0 M_\perp^2$ appears to be valid only for $\tau > 10^3$, whereas $\frac{1}{2}\mu_0 M_s^2$ may be used for $\tau < 1$. For intermediate situations, $1 < \tau < 10^3$, no simple expression for the magnetostatic energy can be given. It depends in a complicated way on the applied field via the (field-dependent) domain size (Kooy and Enz 1960). The saturation fields vary continuously with τ, but the area between the in-plane and perpendicular curves still provides a measure of K_{eff}.

Summarizing, the MAE can in principle be determined from the field dependence of the magnetization by measuring the saturation fields or the area between the in-plane and perpendicular magnetization curves. However, in general, no one-to-one relation exists between the hard-axis saturation field and the total effective magnetic anisotropy energy K_{eff}. The area between the loops, on the contrary, yields K_{eff} in all cases.

In practice, problems are encountered using the 'area method'. For instance, as figure 4 illustrates, the experiments can show a considerable hysteresis and the available field is in some cases not sufficient to saturate the sample in the hard axis direction. In order to determine the MAE in such cases, the hysteresis is removed by averaging the hysteresis loop branches, and the hard axis loop is extrapolated, which is often rather arbitrary for nonlinear curves. These problems can be circumvented by measuring the angular dependence of the magnetization. In this method the applied field is set at a constant value but its angle with respect to the film normal is varied by rotating the sample. During this rotation, the component of the magnetization along the field is measured. The magnetic anisotropy is then determined by fitting the obtained angular dependence by minimization of equation (21). See Bloemen *et al* (1992b) for an example of such a study.

3.2. Magneto-optical Kerr effect measurements

This subsection discusses the use of the MOKE in measuring the magnetic anisotropy. MOKE describes the change in the polarization state of light induced by reflection at the surface of magnetic materials. There are two effects: a rotation of the plane of linear polarization (Kerr rotation) and a change of the ellipticity of the light (Kerr ellipticity). Both originate from a difference in the complex Fresnel reflection coefficients for left and right circularly polarized light. This optical anisotropy is only present for a non-zero magnetization, its magnitude being determined by the off-diagonal terms in the permitivity tensor, which are odd linear functions of the magnetization (Hunt 1967). It is the latter

relation which makes MOKE suitable to study changes in the magnitude or direction of the magnetization. Although no *direct* information can be obtained regarding the absolute magnitude of the magnetization, the angle of Kerr rotation is directly proportional to the magnetization (Suits 1972, Freiser 1968). In addition, since the magnetization is only monitored in that region of the sample which is illuminated by a (focused) light beam (typically 100 μm in diameter, in present studies (Purcell *et al* 1992)), a localized analysis of magnetic behaviour is possible. This allows, for example, a positional scan along a wedge-shaped (magnetic) layer, which enables one to investigate magnetic properties as a function of the layer thickness, in one single sample (see figure 8). A description of a magneto-optical Kerr apparatus and measurement technique has been given by Sato (1981).

In a polar Kerr effect measurement, where the light beam is at normal incidence to the sample, one usually applies the field perpendicular to the sample. The Kerr rotation and the ellipticity in this geometry are proportional to the perpendicular component of the magnetization (Mansuripur 1990). For samples with an in-plane easy axis one obtains a linear increase of the magnetization (and thus of the Kerr signal) up to saturation, as reported in the previous subsection. From the saturation field or anisotropy field one can determine the MAE. However, for samples with a perpendicular easy axis one may obtain a rectangular loop from which the MAE cannot be deduced. In this case the MAE can be obtained in the following way. Application of a field at a non-zero angle with respect to the film normal creates a torque between M and H. The perpendicular component of the magnetization is given by $M_\perp = M_s \cos\theta_{eq}(H)$, and can be calculated relatively easily by solving the equilibrium angle $\theta_{eq}(H)$ from minimization of equation (21) for a given anisotropy. The thus obtained $M_\perp/M_s$ versus H curve can be compared directly with the normalized experimental Kerr signal $S(H)/S_0$, where $S(H)$ and S_0 are the measured Kerr rotations or ellipticities at field H and in zero field, respectively†. A least squares fitting process gives the magnetic anisotropy. Results of such a procedure are the measurements and the corresponding fits shown in figure 6 (Purcell *et al* 1992). A disadvantage of the method is the fact that the Kerr effect does not measure the magnetization directly: the fits only provide the anisotropy *fields*. To obtain the magnetic anisotropy *energy* a value for the saturation magnetization has to be assumed. Usually, experimental accuracies of 10% are obtained. However, this accuracy cannot be obtained for large anisotropies because, in those cases, the drop in the Kerr signal, using the maximum available field, is too low to reliably determine the anisotropy. The latter is best demonstrated in figure 6 by the upper curves. Nevertheless, due to its local character and its monolayer sensitivity, MOKE provides a powerful tool for investigating anisotropies of (single, wedge-shaped) ultrathin ferromagnetic layers.

4. Sample preparation and characterization

Several techniques, developed primarily for the preparation and characterization of ultrathin layers and surfaces, have been adapted over the years to create and study artificial multilayers. Many of these technological advances have originated in the area of layered semiconductors, where quantum well structures prepared from multilayered stacks of two or more semiconducting ultrathin films (such as GaAs and AlGaAs) have found wide application as solid-state lasers or image sensors. In the following, a summary of those techniques which find regular use in the preparation and structural or compositional

† Preceding the measurement, the sample is saturated in a perpendicular field so that one starts with a situation of maximum perpendicular remanence.

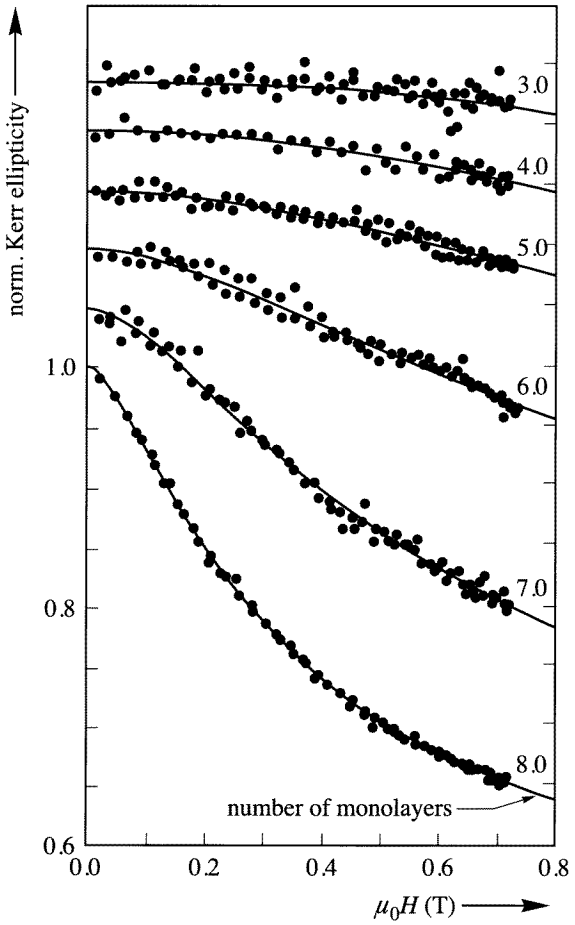

Figure 6. MAE times the Co layer thickness versus the Co layer thickness measured on a wedge-shaped Co layer on Pd(111) using MOKE (full circles). The open squares represent FMR measurements on separate samples with homogeneous Co thicknesses, after Purcell *et al* (1992).

characterization of metallic magnetic multilayers, is given. An illustration of the use may be found in Falicov *et al* (1990).

4.1. Preparation methods

Most magnetic multilayers are prepared by the controlled alternate deposition from two or more metal sources onto a substrate held (mostly at around room temperature) under vacuum conditions to avoid unwanted contamination (evaporation, sputtering, laser ablation deposition). Recently, however, a liquid-phase electrodeposition technique has also proved capable of creating compositionally modulated magnetic multilayers. Some advantages and disadvantages of these more commonly encountered techniques are summarised in table 1.

For good multilayer definition, deposition rates in the order of 0.01–1 Å s^{-1} are generally appropriate.

Table 1. Deposition techniques for preparing magnetic multilayers.

Deposition technique	Advantages	Disadvantages
MBE Low-energy deposition 10^{-10} mbar	Sharp interfaces Low contamination Epitaxy—orientations Atomic beams—wedges Variable alloy compositions	Column formation Island formation Pinholes (Co/Cu(111)) Alloy composition reproducibility Expensive
Sputtering High-energy deposition 10^{-7}–10^{-9} mbar (background) 10^{-3} mbar (sputter gas)	Flat on a 100 nm scale Homogeneity over large areas Reproducible alloy compositions Less pinholes	Diffuse interfaces Some contamination Stresses
Laser ablation Mid-energy deposition 10^{-9} mbar	Strong texture/epitaxy Low contamination Fairly flat on a 100 nm scale	Non-uniform thickness (small substrates) Particles/droplets discrete thicknesses
Electrodeposition	Epitaxy possible Inexpensive	Limited material combinations Conducting substrate Diffuse interfaces Mutual contamination Impurities from solvent

4.1.1. MBE and other evaporation techniques. In molecular beam epitaxy (MBE) and other evaporation techniques, the deposited material is created by thermal evaporation of material from a heated source. This evaporated beam then condenses on the substrate. By using a variety of effusion cell or electron-beam evaporation sources, almost all metals can be evaporated, although the deposition rate for high melting point metals may be rather low (0.1 Å s^{-1}). MBE deposition of alloys requires the simultaneous evaporation (co-evaporation) from separate sources, which places considerable demands on the stability of deposition rates to avoid composition drifting. Of course, many different alloy compositions may be straightforwardly produced by MBE without the requirement of changing sources by merely varying the rates.

In general, MBE produces multilayers with atomically sharp interfaces (0.1 nm scale), coherent epitaxial growth and low contamination, but with roughness on a scale which is large compared to atomic dimensions up to several tens of nm's (convexly curved columns, patches, pinholes). An example of the structure, as obtained in a transmission electron microscope (TEM) cross section, of a MBE-evaporated Co/Au multilayer is given in figure 7.

Substrate temperature and use of buffer or seed layers and the deposition rate are parameters of the evaporation process that can be manipulated. Typical thermal energies of the condensing atoms are 0.1 eV plus any binding energy liberated at the substrate surface. This implies that the surface mobility can be largely controlled with the substrate temperature. A higher substrate temperature (higher surface mobility) was shown to result in wider columns with the convex curvature localized at the boundaries, leaving large flat regions in the middle (Hakkens *et al* 1993). Buffer or seed layers can promote a specific structure or orientation.

The effect on the magnetic behaviour of the sharper interfaces will be to increase the

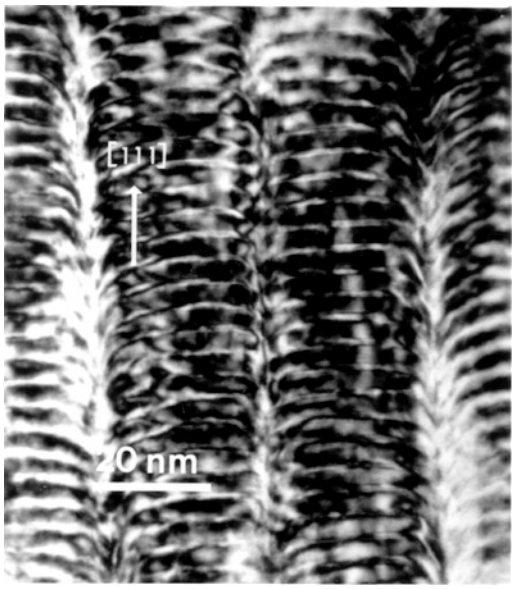

Figure 7. TEM cross section of an evaporated Co/Au multilayer on a 100 nm scale from Hakkens *et al* (1993).

magnetocrystalline interface magnetic anisotropy (favouring a perpendicular easy axis if $K_s > 0$) and the shape magnetic anisotropy (in support of an in-plane easy axis). Due to the columnar structure, however, a spread in the surface normal exists which reduces the two effects just mentioned owing to directional averaging. A correlation between the deposition rate and the magnetic anisotropy was observed by den Broeder *et al* (1992) and was suggested to be related to varying interface diffuseness and magneto-elastic anisotropy contributions.

MBE has shown to be more suited to studies relating structural and magnetic properties to details of the growth process, in general a rather time-consuming activity. An attractive new development is the ability to readily produce (multiple) wedge-shaped samples by partially eclipsing the evaporation beams with a movable shutter (see figure 8), thus saving the preparation of a series of samples with a varying layer thickness. Subsequently, several measurements at different positions on the wedge (different layer thicknesses) may be carried out on a single sample. The wedge technique will be encountered in many of the studies discussed in this review.

4.1.2. Sputter deposition. Sputtering is a very commonly used deposition technique. Electrically accelerated high energy ions (usually from an inert gas) bombard a target material, dislodging and ejecting material which then condenses onto a substrate to form a thin layer. By alternate sputtering of more than one target, a multilayer may be created. Alloys are sputtered from composite targets or alloy targets, however for each alloy composition a separate target must be used. Because of the high ion energies (typically several 10 eV), almost all metals and metallic alloys can be readily sputtered at a relatively high deposition rate (10 Å s^{-1}). The large thickness homogeneity over several cm's makes sputtering also a flexible, frequently employed, industrial fabrication technique. Whilst the higher deposition energies lead to flat multilayers with few grain boundaries or pinholes on

a μm scale, this must be weighed against the interdiffusion created at the interfaces (nm scale).

Sputter process parameters such as sputter pressure, sputtering energy and inert gas element can be varied to modify the structure (Carcia *et al* 1993). These parameters mainly control the stress and, via magnetostriction, the magneto-elastic anisotropy of the multilayers. The stress results from the energy with which the particles in the plasma condense onto or collide with the film. A lower sputtering energy or likewise a higher pressure or a heavier inert gas will all result in less energetic reflected sputter gas neutrals and less energetic sputtered target atoms arriving at the film. In terms of stress this means a change to less compressive or to more tensile stress and, for a positive magnetostriction constant, a promotion of a perpendicular easy axis. Furthermore, these variations of the sputter parameters will give sharper interfaces on a nm scale, but rougher layers with sharp grain boundaries on a μm scale. Consequences of rough interfaces for the magnetic behaviour are opposite to those given above for sharp interfaces. In this respect ion-beam sputtering (IBS) represents a high energy, low pressure form of sputtering resulting in macroscopically (100 nm) flat, but microscopically (1 nm) rough multilayers with diffuse interfaces and compressive stress.

Recently, employment of seed layers has established the possibility of epitaxial growth for sputter deposition of various multilayers, thus allowing growth of other orientations than the closed packed surface (Harp and Parkin 1994, unpublished). In principle, sputtering at low pressures (the multilayer surface-to-shutter distance must be small compared to the mean free path to give a sharp shadow) is also suitable for employing the wedge technique (Bian *et al* 1996).

4.1.3. Laser ablation deposition. In laser ablation deposition (LAD) a pulsed laser is used to vaporize material from (metal) targets, which is subsequently collected onto the sample substrate. The evaporant absorbs laser beam energy and forms a plasma which can be seen near the target. This differentiates LAD from thermal evaporation. For laser ablation small, easily interchangeable targets can be used, making it a flexible technique. Another advantage is the stoichiometric deposition, i.e. the composition of the deposited film will be the same as that of the (compound) target. For metal targets the vaporized particles are

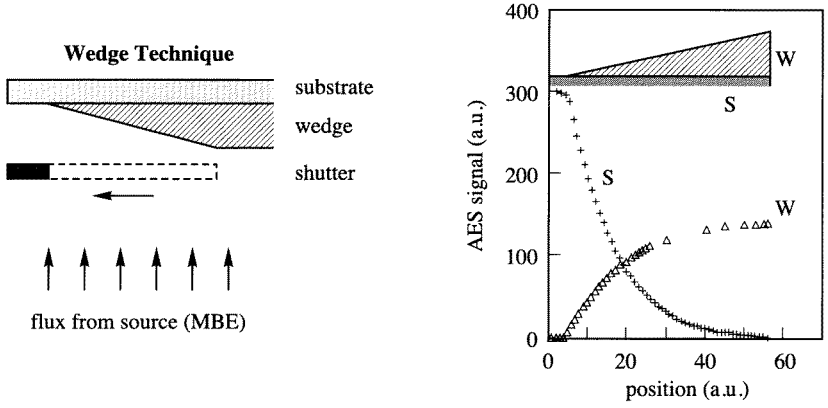

Figure 8. (*a*) Principle of growing a wedge with the help of an eclipsing shutter and (*b*) the Auger electron signals from substrate (S) and wedge (W) as a function of the wedge thickness.

Table 2. *In situ* and *ex situ* structural and compositional characterization techniques.

	In situ	*Ex situ*
Composition and layer thickness	AES/XPS RHEED oscillations Thickness monitors	XRD X-ray fluorescence TEM EPMA/EELS
Structure	RHEED—in-plane LEED—in-plane/perp STM XPS/AES forward scattering (S)EXAFS	XRD HRTEM diffraction/ lattice imaging NMR (Co) CEMS (Fe)

mainly atomic as required for epitaxy. Strongly textured, macroscopically flat multilayers with low contamination can be produced in a relatively inexpensive apparatus. However, problems with thickness non-uniformity, related to the peaked angular distribution of the depositing flux, and the presence of particles, due to droplets in the vaporized plume, have limited the wider use of this technique for magnetic multilayers (Kools 1992, Kools *et al* 1993, Cherief *et al* 1993).

4.1.4. Electrodeposition. In contrast to other techniques used to prepare magnetic multilayers, electrodeposition does not require a vacuum environment: deposition occurs in a solution of metallic ions in an electrolyte by applying an electric potential difference between a metallic substrate and a reference electrode. Although electrodeposition of compositionally modulated films dates from 1930 (Deubner 1930), only in 1986 artificially layered structures with short periods (2–4 nm) were grown (Goldman *et al* 1986). To grow multilayers the metallic substrate is either placed in separate solutions each containing only one of the required constituents or in one solution with two or more metallic species which may be separately deposited by applying different potentials. The first method has the disadvantage of contamination of interfaces during the transport between the solutions, the second method suffers from the contamination of a layer by the accompanying metallic element. In both cases the multilayers will be contaminated with impurities in the solvent. Whilst promising epitaxially grown Co/Cu and Cu/Ni multilayers have been prepared using inexpensive apparatus (Bennett *et al* 1989, McMichael *et al* 1992), it is presently not clear how good the layer thickness control and quality of thin individual layers, and the general applicability of the technique, will be.

4.2. Sample characterization

In table 2, some of the most frequently encountered analysis techniques are listed for the *in situ* and *ex situ* characterization of the structure and composition or layer thicknesses of magnetic multilayers. Most of the *in situ* characterization involves state of the art surface science techniques which have been successfully applied to metallic layers yielding not only information about layer thicknesses, compositions and contamination (Auger electron spectroscopy (AES), see figure 8(*b*), x-ray photo-electron spectroscopy (XPS), quartz crystal thickness monitors), but also about the growth modes encountered (reflection high-energy electron diffraction (RHEED) and RHEED oscillations). Similarly,

the *in situ* structure techniques, providing information such as in-plane (RHEED, low-energy electron diffraction (LEED)) and perpendicular LEED lattice spacings, as well as site-dependent coordination (surface extended x-ray absorption photon spectroscopy ((S)EXAFS)) and symmetry (XPS/AES forward scattering) can nowadays be considered as standard techniques. Scanning tunnelling microscopy (STM) is rapidly becoming an unmissable *in situ* characterization tool, providing direct insight into the topographical roughness of surfaces (from which interface roughness may be inferred) and the growth mode. Obtaining information about buried interfaces is more challenging. Fortunately, two *ex situ* techniques are emerging as extremely suitable methods for providing (statistically averaged) information about interface roughness of magnetic layers: nuclear magnetic resonance (NMR) provides information (roughness, stacking sequence, strains) for Co-containing interfaces, whereas conversion electron Mössbauer spectroscopy (CEMS) provides similar information for ^{57}Fe-containing interfaces. The remaining *ex situ* techniques of x-ray diffraction (XRD) (growth orientation and texture and superlattice peaks for multilayer periods), microscopy (direct multilayer period, see figure 7) and composition analysis with electron probe micro analysis (EPMA), electron energy loss spectroscopy (EELS) and inductively coupled plasma spectroscopy (ICPS) are extremely well established characterization techniques. For complete characterization of the growth, structure and composition of the magnetic multilayers, a wide variety of *in situ* and *ex situ* techniques should be employed (Feldman and Mayer 1986).

5. Overview of anisotropy studies

5.1. Tables

Tables 3, 4 and 5 contain an extensive selection of experimentally observed anisotropy data in Fe-, Co- and Ni-based multilayers.

The fact that, in tables 3, 4 and 5, various (sometimes quite different) numbers for K_s and K_v are cited for one particular system indicates the sensitivity of the anisotropy parameters to growth conditions and structural parameters like interface roughness, strain and orientation. Moreover, actual data on the structural parameters of the layers which have been realized are scarce and generally hard to obtain, or require at the least a series of dedicated experiments. This makes comparison of the results and the search for trends and systematics quite hazardous. Therefore, conclusions drawn from these tables should be considered with care. In this spirit, commentary will be offered in what follows on some of the features apparent from the data presented in the tables. In the next section a few dedicated studies of the influence of growth conditions and structural parameters on the magnetic anisotropy will be discussed.

5.2. Fe versus Ni versus Co

Comparing the observed interface anisotropies, one notes that for Co and Fe these are often positive, i.e. favouring a perpendicular easy direction, whereas for the Ni-based multilayers they are usually negative. There is no simple argument from which one can understand this difference in sign or the fact that a negative K_s should always be the case for Ni. As shown in Daalderop (1991), the MAE is determined by various, largely cancelling contributions which depend on the actual location of the Fermi level and the detailed shape and position of the energy bands. This makes a prediction of the sign of the MAE, without detailed calculation, extremely difficult.

Table 3. Table of out-of-plane interface anisotropies per single interface and volume anisotropies (if given in the article) of sandwiches and multilayers (indicated by a subscript n) containing Fe layers. K_s and K_v are defined positive for favouring a perpendicular easy axis. Substrate, buffer layer and the deposition technique used are indicated (MBE molecular beam epitaxy, E evaporation, IBS, DC-S, RF-S ion beam, direct current, radio frequent sputtering).

Substrate buffer	Composition/ interface	K_s (mJ m^{-2})	K_v (MJ m^{-3})	Deposition technique	Reference
Ag(100)	Fe(100)/UHV	0.96		MBE	Heinrich *et al* (1991a), Cochran *et al* (1988)
W(110), Cr(110)	Fe(110)/UHV	0.97		MBE	Fritzsche *et al* (1994), Elmers and Gradmann (1990)
Ag(100)	Fe(100)/Ag	0.81, 0.69, 0.79		MBE	Heinrich *et al* (1991a)
Ag(100)	Fe(100)/Ag	0.64		MBE	Cochran *et al* (1988)
GaAs(100)	$(Ag(100)/Fe(100))_n$	0.8	−1.2	MBE	Barthélemy *et al* (1992), Cabanel *et al* (1990)
W(110)	Fe(110)/Ag	0.82		MBE	Fritzsche *et al* (1994), Elmers and Gradmann (1990)
Glass, Si	$(Fe(110)/Ag(111))_n$	0.3	−1.2	E	Krishnan *et al* (1992)
Mica/Ag(111)	Fe(110)/Ag	1.45		DC-S	Hurdequint (1991)
Ag(100)	Fe(100)/Au	0.47, 0.40, 0.54		MBE	Heinrich *et al* (1991a)
W(110)	Fe(110)/Au	0.72		MBE	Fritzsche *et al* (1994), Elmers and Gradmann (1990)
Glass/Au(111)	$(Fe(110)/Au(111))_n$	0.51	−1.63	E	Araki *et al* (1989)
Ag(100)	Fe(100)/Cu	0.62		MBE	Heinrich *et al* (1991a)
Si	Fe(110)/Cu	0.32		DC-S	Pechan *et al* (1995)
W(110)	Fe(110)/Cu	0.52		MBE	Fritzsche *et al* (1994), Elmers and Gradmann (1990)
Mica/Cu	Fe(110)/Cu	0.29	−1.3	DC-S	Smardz *et al* (1992)
W(110)	Fe(110)/Cr	0.12		MBE	Fritzsche *et al* (1994), Elmers and Gradmann (1990)
Glass	$(Fe(110)/Mo(110))_n$	0.55	−1.67	RF-S	Obi *et al* (1991)
Ag(100)	Fe(100)/Pd	0.17		MBE	Heinrich *et al* (1991a)
Si/Pd	$(Fe/Pd(111))_n$	0.14	−1.73	E	Draaisma *et al* (1987)
Sapphire	$(Fe(110)/Pd(111))_n$	0.15		S	Hillebrands *et al* (1988)
Glass	$(Fe(110)/Pd(111))_n$	0.30	−1.48	RF-S	Obi *et al* (1991)
	$(Fe/Pd)_n$	0.11		E	Luykx *et al* (1988)
Si(111)	$(Fe(100)/Pt(100))_n$	0.47 ($t_{Fe} < 8$ Å)	−2.8 ($t_{Fe} < 8$ Å)	E	Sakurai (1994)
Si(111)	$(Fe(100)/Pt(100))_n$	−0.31 ($t_{Fe} > 8$ Å)	−1.7 ($t_{Fe} < 8$ Å)	E	Sakurai (1994)
W(110)	W/Fe(110)	−1.92		MBE	Fritzsche *et al* (1994), Elmers and Gradmann (1990)

The tables do not show the thicknesses $t_\perp$ at which the multilayers change their preferential orientation from perpendicular to along the film plane. Typical values for Co-based multilayers are in the range of 0–25 Å (Engel *et al* 1991a), depending on the non-magnetic metal and the structural quality of the layers. For Fe-based systems, the observed values for $t_\perp$ are generally smaller, notwithstanding the often larger positive interface anisotropies. This is mainly due to the shape contribution, which is larger for the Fe layers because of the higher saturation magnetization, and to the absence of significant bulk magnetocrystalline contributions.

Table 4. Table of out-of-plane interface anisotropies per single interface and volume anisotropies (if given in the article) of sandwiches and multilayers (indicated by a subscript n) containing Co layers. K_s and K_v are defined positive for favouring a perpendicular easy axis. Substrate, buffer layer and the deposition technique used are indicated (MBE molecular beam epitaxy, E evaporation, IBS, DC-S, RF-S ion beam, direct current, radio frequent sputtering).

Substrate buffer	Composition/ interface	K_s (mJ m^{-2})	K_v (MJ m^{-3})	Deposition technique	Reference
Glass/Au(111)	Co(111)/UHV	−0.28			Ould-Mahfoud *et al* (1993)
Glass/Au(111)	Co(0001)/UHV	−0.17			Beauvillain *et al* (1994)
Cu(100)	Co(100)/UHV	−1.06		MBE	Krams *et al* (1992)
W(110)/Pd	Co(0001)/UHV	−0.28		MBE	Kohlhepp and Gradmann (1995)
W(110)/Pd	Co(0001)/Ag	0.24		MBE	Kohlhepp and Gradmann (1995)
Glass/Ag	$(Co/Ag)_n$	0.20, 0.30	−0.97	E	den Broeder *et al* (1991)
Glass,Si/Ag	$(Co/Ag)_n$	0.16	−0.93	E	Krishnan *et al* (1992)
Si(100)	$(Co/Al)_n$	0.25	−0.76	E	Mitsuzuka *et al* (1990)
Sapphire	$(Co/Au(111))_n$	0.07	−0.77, −0.98	MBE	Kingetsu and Sakai (1993)
Cu(111)	Co/Au(111)	0.37		MBE	Kohlhepp *et al* (1992)
Glass/Au	$(Co/Au(111))_n$	0.42	−0.43	E	Takahata *et al* (1989)
Glass/Au	$(Co/Au(111))_n$	0.58	−0.70	E	den Broeder *et al* (1991)
Glass/Au	$(Co/Au(111))_n$	0.42	−4.34	E	Araki *et al* (1989)
Glass/Au	Co/Au(111)	0.53		E	Chappert and Bruno (1988)
Glass/Au	Co/Au(111)	0.56	−0.75	E	Grolier *et al* (1993)
Si/Au	$(Co/Au(111))_n$	0.45		IB-S	den Broeder *et al* (1988)
	Co/Au	1.28			Lamelas *et al* (1989)
	$(Co/Au)_n$	0.34	−0.73	E	Sakurai *et al* (1991)
Cu(100)	Co(100)/Cu	0.15		MBE	Krams *et al* (1992)
Cu(100)	Co(100)/Cu	0.15	−1.2		Hillebrands *et al* (1994)
Cu(110)	Co(110)/Cu	−0.86	Various		Fassbender *et al* (1995), Hillebrands (1966)
Cu(111)	Co(111)/Cu	0.21	−0.9		Hillebrands *et al* (1994)
Sapphire	$(Co/Cu(111))_n$	−0.02	−1.19	DC-S	England *et al* (1988)
Cu(111)	Co/Cu(111)	0.18		MBE	Kohlhepp *et al* (1992)
	Co/Cu	0.53			Lamelas *et al* (1989)
Glass/Cu	$(Co/Cu)_n$	0.10, 0.12	−0.8	E	den Broeder *et al* (1991)
Glass/Ir	$(Co/Ir)_n$	0.8	−1.20	E	den Broeder *et al* (1991)
Glass/Mo	$(Co/Mo)_n$	0.3, 0.2	−0.84, −0.87	E	den Broeder *et al* (1991)
Cu(100)	Ni/Co/Ni(100)	0.23		MBE	Johnson *et al* (1992)
Cu(110)	Ni/Co/Ni(110)	0.19		MBE	Johnson *et al* (1992)
Cu(111)	Ni/Co/Ni(111)	0.42		MBE	Johnson *et al* (1992)
Glass,Si/Au	$(Co/Ni(111))_n$	0.31		E	Daalderop *et al* (1992)
Glass/Au	$(Co/Ni(111))_n$	0.20		E	den Broeder *et al* (1992)
Glass,Si,Mica	$(Co/Ni)_n$	0.19–0.24		E	Bloemen *et al* (1992a)
	$(Co/Ni)_n$	0.1		E	Luykx *et al* (1988)
	Co/Os(111)	0.7	−0.90		Bloemen (unpublished)
NaCl/Pd	$(Co/Pd(100))_n$	0.32	−2.19	E	den Broeder *et al* (1989)
GaAs	$(Co/Pd(100))_n$	0.63	−4.50	MBE	Engel *et al* (1991a)
GaAs	$(Co/Pd(110))_n$	0.63	−1.82	MBE	Engel *et al* (1991a)
W(110)/Pd	Co(0001)/Pd	0.65		MBE	Kohlhepp and Gradmann (1995)
Pd(111)	Co/Pd	0.92	−1.00	MBE	Purcell *et al* (1992)
Si/Pd	$(Co/Pd(111))_n$	0.26	−0.72	E	Draaisma *et al* (1987)
Glass/Pd	$(Co/Pd(111))_n$	0.40, 0.56	−0.86	E	den Broeder *et al* (1991)
Mica/Pd	$(Co/Pd(111))_n$	0.58, 0.74	−0.91	E	den Broeder *et al* (1991)
Glass/Pd	$(Co/Pd(111))_n$	0.25, −0.31	−0.64, −0.80	DC-S	Hashimoto *et al* (1989)
Glass,Kapton	$(Co/Pd(111))_n$	0.16		RF-S	Carcia *et al* (1985)
	$(Co/Pd(111))_n$	0.5	−1.2	E	Sakurai *et al* (1991)

Table 4. (Continued)

Substrate buffer	Composition/ interface	K_s (mJ m^{-2})	K_v (MJ m^{-3})	Deposition technique	Reference
GaAs	$(Co/Pd)_n$	0.63	−0.50	MBE	Engel *et al* (1991a)
	Co/Pd	0.35	−1.08	E	Luykx *et al* (1988)
GaAs	$(Co/Pt(100))_n$	0.59	−5.98	MBE	Weller *et al* (1993)
Glass, Quartz, Si/Pt	$(Co/Pt(100))_n$	0.31	−1.00	E	Lin *et al* (1991)
GaAs	$(Co/Pt(110))_n$	0.42	−1.95	MBE	Weller *et al* (1993)
Glass, Quartz, Si/Pt	$(Co/Pt(110))_n$	0.37	−0.91	E	Lin *et al* (1991)
Glass, Quartz, Si/Pt	$(Co/Pt(111))_n$	0.76	−0.92	E	Lin *et al* (1991)
GaAs(111)	$(Co/Pt(111))_n$	0.82		MBE	Lin *et al* (1991)
GaAs	$(Co/Pt(100))_n$	0.20	−0.73	E	Harzer *et al* (1992)
Glass,Si	$(Co/Pt(111))_n$	0.42	−0.68	E	Zeper and Carcia (1989)
Glass/Pt	$(Co/Pt(111))_n$	0.50, 0.58	−1.0, −0.7	E	den Broeder *et al* (1991)
Si	$(Co/Pt(111))_n$	0.27	−0.7	E	Harzer *et al* (1992)
GaAs	$(Co/Pt(111))_n$	0.97	−0.74	MBE	Weller *et al* (1993)
	$(Co/Pt(111))_n$	0.92	−1.11	S	Weller *et al* (1993)
Pt(111)	Co/Pt	1.15	−0.77	MBE	McGee *et al* (1993)
	$(Co/Ru)_n$	0.4	−0.45	E	Sakurai *et al* (1991)
Mica/Ru	$(Co/Ru)_n$	0.5	−0.68	E	Dinia *et al* (1992)
Sapphire	$(Co/Ti)_n$	0.23	−0.92	DC-S	van Leeuwen *et al* (1990)
	Co/V	1.05	−1.1		Bloemen (unpublished)
W(110)	Co(0001)/W	−0.3, −0.6		MBE	Fritzsche *et al* (1995)
Mica/Ru	$(Co/Cr(110))_n$	0.64	−0.98	E	Henry *et al* (1993)

Inspection of tables 3, 4 and 5 shows that a rather broad range of values of K_v is reported. The main contribution to K_v is the shape anisotropy, which amounts to −1.86, −1.27 and −0.14 MJ m^{-3} for Fe, Co and Ni, respectively. In the case of Co, however, there may be an additional magnetocrystalline anisotropy: for bulk fcc Co it is negligible and for bulk hcp Co it equals 0.53 MJ m^{-3} at room temperature (Landolt-Börnstein 1986). In layered systems, both hcp Co and fcc Co can be stabilized at room temperature. Without magneto-elastic contributions, one therefore expects $K_v = -1.27$ MJ m^{-3} (fcc Co) or $K_v = -0.74$ MJ m^{-3} (hcp Co), thus generally giving a larger $t_\perp$ for Co layers with a hexagonal structure. Comparison with table 4 shows important deviations which are generally attributed to strain or mixtures of hcp and fcc phases (van Alphen *et al* 1993). In particular, a strain contribution is invoked in order to explain K_v values outside the range spanned by the hcp and fcc K_v values. Deviations of K_v of Fe and Ni are also ascribed to strain.

The size of table 4 compared to 3 and 5 reflects to some extent the industries preferential interest in multilayers based on Co compared to Fe and Ni.

6. Influence of the structure on the magnetic anisotropy

In the discussion of the experimental results, it should be realized that the structure of the magnetic layers is extremely important for the actually observed magnetic anisotropies. The importance of the topology of the interfaces and of the crystallographic structure of the magnetic layers was already mentioned. The structural properties are strongly determined by the complex interplay between the employed growth technique (e.g. sputtering, evaporation, laser ablation), the preparation conditions (temperature, growth rate, sputtering pressure), the elements which are grown, their thicknesses and lattice mismatch, the symmetry,

Table 5. Table of out-of-plane interface anisotropies per single interface and volume anisotropies (if given in the article) of sandwiches and multilayers (indicated by a subscript n) containing Ni layers. K_S and K_V are defined positive for favouring a perpendicular easy axis. Substrate, buffer layer and the deposition technique used are indicated (MBE molecular beam epitaxy, E evaporation, IBS, DC-S, RF-S ion beam, direct current, radio frequent sputtering).

Substrate buffer	Composition/ interface	K_s (mJ m^{-2})	K_V (MJ m^{-3})	Deposition technique	Reference
Re(0001)	Ni(111)/UHV	−0.48		MBE	Gradmann *et al* (1984)
Mica/Ag	$(Ni/Ag(111))_n$	−0.04	0.003	E	Chubing *et al* (1992)
Si(100)	$(Ni/Au(111))_n$	−0.15		DC-S	Childress *et al* (1992)
NaCl	$(Ni(100)/Cu(100))_n$	−0.23		DC-S	Xiao and Chien (1987)
Cu(100)	Ni/Cu	−0.4	0.39, −0.16	MBE	Jungblut *et al* (1994)
Cu(100)	Ni/Cu	−0.17	0.35	MBE	Schulz and Baberschke (1994a), Schulz *et al* (1994b)
Cu(111)	Ni/Cu	−0.08	0.13, −0.19	MBE	Jungblut *et al* (1994)
Re(0001)	Ni(111)/Cu	−0.22		MBE	Gradmann *et al* (1984)
Mica/Cu	$(Ni(111)/Cu)_n$	−0.3		E	Gyorgy *et al* (1980)
Mica/Cu	$(Ni(111)/Cu)_n$	−0.12		DC-S	Xiao and Chien (1987), Gyorgy *et al* (1980)
Mica	$(Ni/Mo)_n$	−0.11, −0.54		DC-S	Pechan and Schuller (1987)
Re(0001)	Ni(111)/Pd	−0.22	−0.010, −0.006	MBE	Gradmann *et al* (1984)
Glass	$(Ni/Pd(111))_n$	0		E, DC-S	den Broeder *et al* (1991)
Glass	$(Ni/Pd)_n$	0.51		RF-S	Maksymowicz and Jankowski (1995)
Mica	$(Ni/Pd)_n$	0.26		RF-S	Maksymowicz and Jankowski (1995)
Re(0001)	Ni(111)/Re	−0.19		MBE	Gradmann *et al* (1984)

lattice spacing and quality of the substrate and the resulting growth mode (layer by layer, Volmer–Weber, Stranski–Krastanov). In the following two subsections the effect of interface roughness and interdiffusion and the effect of strain in the coherent and incoherent growth regime will be discussed.

6.1. Effect of roughness and interdiffusion

So far, it was tacitly assumed that the layers have ideal flat interfaces. In practice, films cannot be grown perfectly. Roughness and/or interdiffusion will be present and will modify the magnetic properties. Here, a brief comment will be made on their effects on the magnetic anisotropy.

6.1.1. Theory. The effect of roughness on the *dipolar* anisotropy has been studied theoretically by Bruno (1988a). A rough surface can be characterized by the roughness ζ, which is the mean square deviation from the ideally flat surface, and the correlation length ξ, the average lateral size of flat areas on the surface (terraces). Roughness creates in-plane demagnetizing fields at the edges of terraces, thereby reducing the shape anisotropy. The anisotropy contribution resulting from the roughness will, therefore, always be positive (favouring PMA). In addition, due to its presence at the interfaces only it will scale as $1/t$. The magnitude of the corresponding dipolar interface anisotropy is a complicated function of ζ and ξ, which can be found in (Bruno 1988a). Under 'normal' conditions ($\zeta = 2$–4 Å, $\xi = 20$ Å) however, the contribution appears to be small (≈ 0.1 mJ m^{-2} for Co(0001)).

Roughness also introduces step atoms at the interface. It has been derived (Bruno 1988b), using the pair interaction model, that these step atoms should reduce the interface

anisotropy contribution of *magnetocrystalline* origin. The extent of this reduction will be determined by the change of the anisotropy of the step atoms relative to terrace atoms and by the number of step atoms relative to the number of terrace atoms. The former depends on the geometry of the interface; the latter is determined by the height of the steps ζ, their length ξ and the number of steps per unit length ($1/\xi$). Bruno (1988b) has derived that the relative reduction in K_s for a simple cubic (100) interface is given by $\Delta K_s/K_s = -2\zeta/\xi$, which can be substantial (20% for $\zeta = 2$ Å and $\xi = 20$ Å). This prediction has been quantified in a series of elegant experiments on Fe/Au multilayers (Lugert *et al* 1993).

As mentioned, interdiffusion might occur during the deposition of the layers. It is clear that diffuse interfaces introduce randomness in the magnetic pair bonds according to Néel's model, which obviously reduces the interface anisotropy. Draaisma and de Jonge (1988) have paid attention to this problem and have demonstrated via calculations based on the pair interaction model a strong dependence of K_s on the degree of mixing.

Although the application of the pair interaction model in the latter two cases demonstrated the importance of the topology of the interface, it would be interesting to compare the results with the outcome of more advanced calculations such as in (Daalderop 1991). The first calculations of this type predict a reduction in magnetocrystalline anisotropy resulting from the presence of defects (MacLaren and Victora 1994).

6.1.2. Experiments. It is worth noting that the interface anisotropies observed for samples grown on single crystals are generally larger than those observed for polycrystalline samples. This indicates the importance of the interface quality. Examples expressing this are a study on Co/Au multilayers (den Broeder *et al* 1988) and work on a wedge-shaped Co layer (Purcell *et al* 1992). In the experiment with the Co/Au multilayers, the samples were prepared by IBS, resulting in rather diffuse interfaces due to the Ar-ion bombardment during growth. The interface quality was manipulated by an annealing treatment before and after which the anisotropy was measured. The results rendered in figure 9 show a drastic increase of K_s after heat treatment. This increase in K_s, accompanied by a strong increase of the intensity of the multilayer reflections observed in XRD experiments, was interpreted as due to a sharpening of the Co/Au interfaces.

In the experiments on a Co wedge (Purcell *et al* 1992), an attempt was made to study the magnetic anisotropy in a Co/Pd bilayer grown as ideally as possible on a Pd(111) single crystal. The use of a Co wedge ensured identical preparation conditions for each Co thickness. Positional scans along the wedge using the Kerr effect yielded the magnetic anisotropies. The results are depicted in figure 10. Note that the interface anisotropy (0.92 mJ m^{-2}) and the thickness range (0–18 Å) for which perpendicular magnetization occurs are significantly larger than observed for polycrystalline Co/Pd(111) multilayers (compare table 4 and figure 2). Unfortunately, few studies of this type have been performed so far. Apart from their relevance from the fundamental point of view, they also yield an upper limit for the best achievable properties, which is of importance for application-oriented research.

6.1.3. Non-linear Kt versus t behaviour. Figure 9 shows a deviation from the linear behaviour at small Co thicknesses. This feature is often encountered in the anisotropy studies of transition metal multilayers. Apart from a possible coherent–incoherent transition, with the accompanying changes in the magneto-elastic anisotropy contributions as discussed in subsection 2.3, several explanations can be given. Assuming, for instance, that at small Co thickness the film is no longer a continuous flat layer but is broken up into

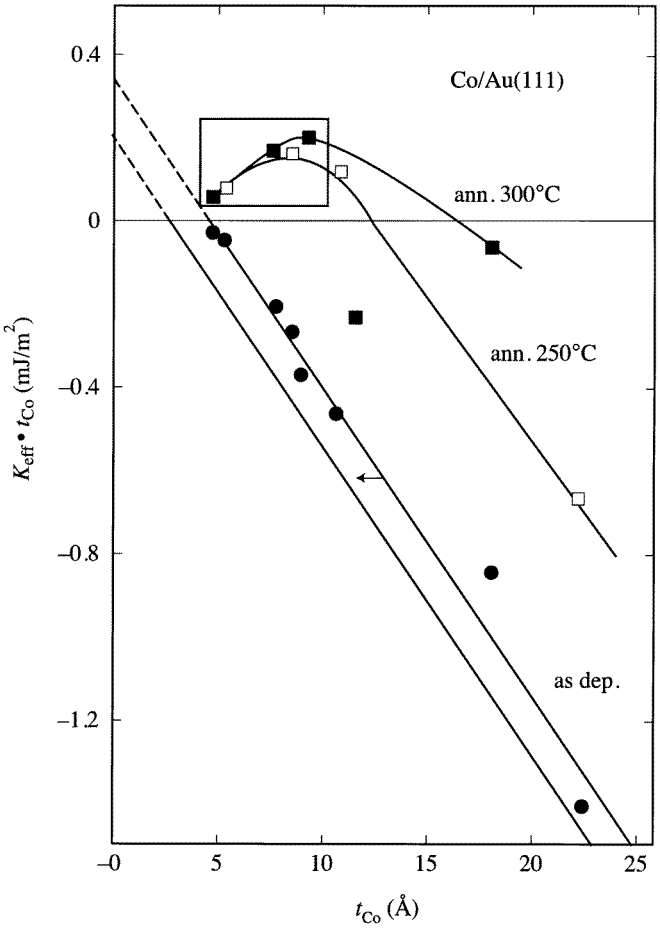

Figure 9. MAE times the Co layer thickness versus the Co layer thickness for ion-beam sputtered Co/Au multilayers before and after annealing at 250 °C and 300 °C (den Broeder *et al* 1988).

islands, necessarily yielding a lower effective magnetic/non-magnetic interface area, a lower interface contribution and a correspondingly lower total anisotropy than expected from the relation $K_{\mathrm{eff}} = K_{\mathrm{v}} + 2K_{\mathrm{s}}/t$. Apart from interdiffusion, which can also account for nonlinear behaviour if the magnetic-layer thickness becomes comparable to the thickness of the diffusion zone, a lowering of the Curie temperature with the magnetic layer thickness, which is a well known finite-size effect, can also play a role in the case of room temperature measurements (Bloemen *et al* 1991). Moreover, one should realize that for ultrathin magnetic layers it is not at all apparent that one is allowed to separate the MAE into interface and volume contributions, a remark already made in section 1.

6.2. Magneto-elastic effects

The data, as presented in tables 3, 5 and 4, give, as such, no direct clue about the physical background. K_{v} and K_{s} may, as seen before, include contributions of magnetic dipolar, magnetocrystalline and magneto-elastic origin. In general, the latter contribution has naturally been interpreted as a volume contribution to the magnetic anisotropy, the strain

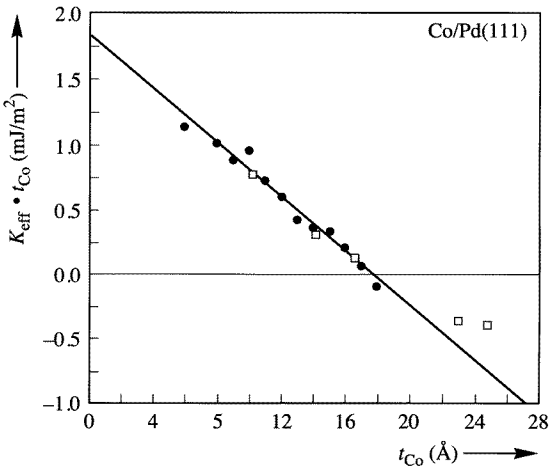

Figure 10. Measurements of the polar Kerr ellipticity at various Co thicknesses along a Co wedge, sandwiched between Pd, with the applied field at an angle of 60° with respect to the film normal. The full line represents fits using first- and second-order anisotropy constants, after Purcell *et al* (1992).

being present throughout the sample. In the case of epitaxially grown multilayers with a lattice misfit between the constituents, as outlined in subsection 2.3, the particular form of strain encountered has been proposed to contribute not only to K_v (coherent growth regime), but also to K_s (incoherent growth regime).

To analyse the data, one of the crucial tasks is thus to determine whether or not the layers are incoherent. The observation of a coherent–incoherent transition at t_c, see figure 3(*b*), might of course be indicative but, as was mentioned before, other mechanisms may also induce such nonlinear behaviour. Another possibility is to rely on a theoretical prediction for t_c. Although the specific numbers depend on the geometry of the multilayer system, it appears that for Co/X multilayers with a large mismatch, such as Co/Au and Co/Pd ($\eta = 0.15$ resp. $\eta = 0.09$), a t_c of at most 2 or 4 Å is predicted (van der Merwe 1963). Consequently, incoherent behaviour in the complete thickness range is expected. For Co/Cu or Co/Ni multilayers ($\eta = 0.02$ resp. $\eta = -0.01$), t_c is much larger, and coherent behaviour might be anticipated. Calculations of the strain and the magneto-elastic anisotropy, based on expressions given in subsection 2.3 show, in some cases, that magneto-elastic contributions to K_s could be expected to be in the same range (sign and magnitude) as the experimentally observed data: Co/Au (Chappert and Bruno 1988), Co/Pd (den Broeder *et al* 1991). On the other hand, dedicated experiments in Ni/Pd and NiFe/Pd multilayers demonstrated a marked disagreement between the expected magneto-elastic contribution and the experimental data (den Broeder *et al* 1991).

Direct observations of the strain are not consistent with expectations in all cases. As expected, in the case of Co/Pd an almost immediate relaxation towards the bulk lattice spacing was concluded from RHEED (Purcell *et al* 1991) and TEM (Hakkens *et al* 1992) experiments. For Ni grown on Cu(100) the expected behaviour was observed too (Bruno and Renard 1989). In NMR experiments measuring the strain in Co/Ni and Co/Cu multilayers as a function of the Co and Ni or Co and Cu layer thickness, a coherent growth consistent with theoretical predictions was found for Co/Ni multilayers. However, the observations on Co/Cu multilayers did not fully agree with the expected behaviour (de Gronckel *et al* 1992,

van Alphen *et al* 1994).

In a few studies the actually observed strain is used to calculate the magneto-elastic anisotropy, but various research groups have come to quite opposite conclusions. In a pioneering experiment, Gradmann (1966) noted that tensile stresses in the Ni layers of Cu/Ni sandwich structures were responsible for the appearance of PMA at certain Ni layer thicknesses, but could not explain the reappearance of in-plane magnetization for thinner Ni layers. More recently, Lee *et al* (1990) explained the thickness dependence of the anisotropy for Co/Au and Co/Cu multilayers as being due solely to Co-layer misfit strain variations. In addition, Nakamura *et al* (1991) also considered that, in sputtered Co/Pd multilayers, PMA is caused mainly by interfacial strain anisotropy of interface alloys. Awano *et al* (1988) reported that the calculated stress-induced anisotropy is 10–100 times smaller than the measured values of the magnetic anisotropy. On the other hand, in a series of experiments on Co/Pd multilayers with various crystal orientations, the K_v values could be fully accounted for by magneto-elastic and magnetocrystalline anisotropy contributions, suggesting that K_s was only due to Néel-type anisotropy (Engel *et al* 1991a). This unclear situation regarding the role of K_N and K_{me} is probably related to the large lattice misfit in most of the studied systems, precipitating immediate incoherent growth which excludes distinct identification of K_N and K_{me}. Below an investigation of the Néel-type and magneto-elastic interface anisotropy of a Cu/Ni/Cu sandwich with a small lattice mismatch and a large t_c is discussed.

6.2.1. MBE-grown Cu/Ni/Cu in (100) and (111) orientations. An inverse proportionality of strain to layer thickness, similar to that experimentally observed in, for example, Ni overlayers on a Cu(100) substrate (Matthews and Crawford 1970), will have important consequences for the interpretation of the anisotropy as outlined below. Both Néel and misfit interface anisotropies are found to be active in determining the magnetic anisotropy in Cu/Ni/Cu sandwich structures. The change of misfit strain with increasing Ni layer thickness from a coherent to an incoherent regime could be followed in samples with a Ni wedge structure and related to changes in the anisotropy, making it possible to quantify the contribution of strain to both K_s and K_v. The majority of the structural and magnetic properties were determined from measurements on only two Cu/Ni wedge/Cu samples, one in the (100) and the other in the (111) crystallographic orientation (Jungblut *et al* 1994).

Structural measurements were directed towards identifying the onset of strain relaxation in the Ni layer. Perpendicular and in-plane Ni lattice spacings were determined using LEED as a function of Ni coverage on Cu. Initially, the Ni displayed a fcc surface net which was nearly identical to that of the Cu substrate. Strain relaxation manifested itself in the LEED patterns through the occurrence of additional features located close to the primary diffraction spots, caused by diffraction from regular arrays of dislocations at large repeat intervals ($\simeq a/\eta$) (Purcell *et al* 1993). To evaluate the agreement between these observations and theory, equation (13), applied to the single layer situation actually encountered in the LEED measurements, is considered. Using literature values for the (orientation-dependent) elastic and shear moduli for Ni (Smithells 1976), and $b = 2.5$ Å ([110] slip direction), one expects $t_{c,(111)} = 11$ Å and $t_{c,(100)} = 13$ Å, see table 6. The close agreement between predicted and observed critical thicknesses in both orientations makes the thermodynamically limited formation of dislocations plausible, and lends credence to the prediction of the critical thicknesses in the case of a sandwich. The transition from elastic strain ($t < t_c$) to strain relaxation ($t > t_c$) plays an important role in determining the anisotropies of the samples.

The results of the anisotropy study appear in figure 11, where the form of both curves strongly resembles the schematic depiction in figure 3(*b*). Clear breaks are observed in both

Table 6. Summary of Cu/Ni anisotropy data pertaining to both investigated orientations. Critical thicknesses, t_c, reported for both single layers and sandwiches, and stress induced anisotropy energies are determined both experimentally and, in parentheses, by calculation.

	t_c (Å)		$t < t_c$		$t > t_c$		K_{me}	
Orientation	Layer	Sandwich	K_s (mJ m^{-2})	K_v (MJ m^{-3})	K_s (mJ m^{-2})	K_v (MJ m^{-3})	$K_{me,s}$ (mJ m^{-2})	$K_{me,v}$ (MJ m^{-3})
(111)	13 (11)	32 (35)	−0.08	0.13	0.27	−0.09	0.35 (0.64)	0.22 (0.36)
(100)	15 (13)	42 (40)	−0.40	0.39	0.90	−0.16	1.30 (0.80)	0.55 (0.39)

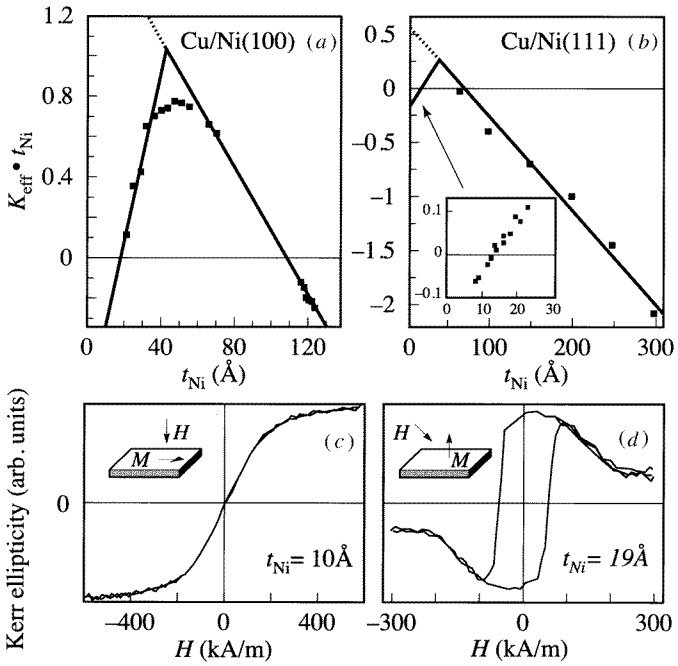

Figure 11. MAE K times the Ni layer thickness t, plotted as a function of t for (*a*) (100) and (*b*) (111) orientations. Kerr hysteresis loops from which the in-plane or perpendicular anisotropy was determined for the (111) oriented sample for Ni thicknesses of (*c*) 10 Å and (*d*) 19 Å, after Jungblut *et al* (1994). Full lines represent linear fits yielding the values of K_v and K_s in table 6.

curves. By comparing the positions of these kinks to the predicted t_c values for sandwich structures (see table 6), a remarkably good agreement is found for both orientations. In the spirit of figure 11, one can straightforwardly assert a linear dependence of $K_{eff}t$ on t, both below and above t_c. The resulting anisotropies are also compiled in table 6. Comparing equations (17) and (18) with (19) and (20), respectively, values for the strain-related interface anisotropy ($K_{me,s}$) and volume anisotropy ($K_{me,v}$) are easily derived. These are also compiled in table 6 (assuming $K_{mc} = 0$ MJ m^{-3} for Ni). Using the relevant magnetostriction and elastic constants in these equations ($\lambda_{100} = -46 \times 10^{-6}$ and $\lambda_{111} = -24 \times 10^{-6}$), the theoretical values of K_{me} can be determined. As shown in table 6, the predicted volume and interface strain anisotropies all have the correct magnitude and sign to account for the experimental observations.

Investigation of these MBE-grown Cu/Ni/Cu samples has allowed isolation of the Néel- and misfit-type anisotropies, which have previously eluded separation, because several favourable conditions are met. First, both metals are fcc with only a small lattice misfit. Consequently, as revealed by the LEED studies, both coherent and incoherent structures can be realized over a wide range of Ni thicknesses accessible to anisotropy measurements. In addition, the small saturation magnetization of Ni (compared to Co or Fe) results in a domination of strain-induced anisotropies over shape anisotropy. Finally, magnetocrystalline anisotropies are rather small in Ni.

A recent FMR investigation of a (100) oriented Ni film grown on a Cu substrate confirmed the role of the misfit interface anisotropy (Schulz and Baberschke 1994). Identical behaviour was found to that of the presented Cu/Ni wedge/Cu(100) samples (Jungblut *et al* 1994), with the magnetization crossing from in-plane to perpendicular and back into the plane with increasing Ni thickness. Below t_c, an almost identical (strain-induced) K_v (0.44 MJ m^{-3}) but slightly different K_s (-0.2 mJ m^{-2}) were reported, compare with table 6. As only a single Cu/Ni interface was present, the reduced (in-plane) interface anisotropy contribution of the thin Ni film (Schulz and Baberschke 1994) resulted in a transition to perpendicular magnetization at a smaller Ni thickness (10 Å) than in the Cu/Ni wedge/Cu sample (18 Å, see figure 11(*a*)). Presumably, the break in the anisotropy should also occur at a lower thickness in the thin film than in the sandwich sample (as a result of the reduced t_c of the thin film). Unfortunately, this was not investigated in detail, although from the limited data the break appears to occur between 15 Å and 40 Å, in any case at a smaller Ni thickness than in the sandwich structures (42 Å, see figure 11(*a*)). Concerning the cross-over from perpendicular to in-plane anisotropies at larger Ni thicknesses, the present results are seen to be consistent with the work of Chang (1990). There, a reversal of the magnetic anisotropy was measured for Ni layers sandwiched between thick Cu(100) layers which occurred at a Ni thickness in between 50 Å (perpendicular remanence) and 100 Å (in-plane remanence). In their attempt to explain the anisotropy of Co/Pd multilayers by magneto-elastic anisotropy of interface alloys, Nakamura *et al* (1991) found similar kinks in the anisotropy of $Pd_{67}Co_{33}$/Au and $Pd_{67}Co_{33}$/Cu multilayers. This behaviour is suggested to be related to the strain-relaxation mechanism proposed here.

7. Orientational dependence of the perpendicular magnetic anisotropy

Extending our understanding of perpendicular magnetic anisotropy (PMA) beyond the phenomenological approach of volume- (K_v) and interface-anisotropies (K_s) requires caution. Experimentally, many factors such as roughness, formation of interface alloys, or patchiness of ultrathin layers may cause a reduction in PMA. Where stresses are present in multilayer growth, these may, under particular circumstances, contribute to both K_v and K_s (subsection 2.3), as demonstrated for the Cu/Ni/Cu system (see subsection 6.2). Theoretically, the difficulty in modelling incoherently grown materials prevents a detailed quantitative comparison with most experimental systems. Therefore, an evaluation of the underlying approximations common to all of the theoretical quantitative studies becomes very difficult.

Of the theoretical predictions which may be tested experimentally, perhaps the most important are the electronic structure effects on PMA and their associated orientational dependence. Originally, Néel discussed the anisotropy within a pair interaction model (Néel 1954), the reduced symmetry at the interface resulting in anisotropies differing greatly from that of the bulk, which were furthermore predicted to be orientationally dependent. Such a simple pair model is, however, less suited to transition metal multilayers, where the itinerant

electron model is more appropriate.

In this section, the orientational dependence of the PMA is discussed for a wide variety of Co and Ni based systems: Co/Pt, Co/Pd, Co/Ni, Co/Cu and Cu/Ni. The inherent sensitivity of the interface anisotropy to differences in interface quality associated with the various available preparation techniques (see sections 4 and 5) necessitates a stringent selection of the samples in which it may be possible to identify orientational effects related to the electronic structure and not merely variations in the interface quality. Consequently, all the samples considered have been prepared at relatively low temperatures by MBE, to minimize the effects of interface roughness (on the atomic level) and interdiffusion, which may result in the formation of ordered or disordered interfacial alloys. Emphasis has been given, where possible, to series of samples prepared by the same groups—this in order to further reduce experimental uncertainties (discussed below), which tend to reduce the observed K_s values.

7.1. Structural aspects

The similarity of the preparation technique (MBE in all cases) does not, however, result in a uniformity in the growth of the different samples: the differences in lattice mismatch, orientation and thicknesses encountered ensure that widely different growth modes—from completely coherent epitaxy, through samples displaying a transition from coherent to incoherent growth, to incoherent growth—are encountered. The consequences of the different growth modes in identifying an interface anisotropy of purely electronic origin will first be considered for individual systems, after which the orientational dependence of the PMA and its relationship with first-principles calculations may be discussed.

7.1.1. Co/Pt and Co/Pd—seeded epitaxy. Both Co/Pt and Co/Pd hcp/fcc systems display equivalently large lattice mismatches of around 9%, which result in a rather similar growth behaviour. Extensive structural characterization, using LEED, RHEED, AES and angle-resolved XPS ('forward scattering'), has been carried out on the initial growth of Co/Pd and Co/Pt in the (111) orientation (McGee *et al* 1993, Purcell *et al* 1993). Both systems grew epitaxially and incoherently, with the in-plane Co lattice constants relaxing to close to the bulk value within the first monolayer. The initial growth was not perfect layer-by-layer growth as some minor island formation was encountered, whilst no indication of interdiffusion was found using angle-resolved XPS. At somewhat larger Co thicknesses (above 4–5 Å), extra diffraction features around the main Co LEED spots attested to a periodic modulation of the Co lattice as a result of the incoherent epitaxy on the Pt or Pd substrates, see figure 12(*a*). It has recently been established using the STM technique that this modulation is associated with a small periodic variation of the perpendicular spacing of the Co atoms on a Pd(111) substrate, see figure 12(*b*) (Kohlhepp and Jungblut unpublished). LEED studies, however, indicated that these thicker Co layers exhibited average perpendicular lattice spacings identical, within experimental uncertainty, to that of bulk Co.

Similar behaviour was reported for (111) oriented multilayers of Co/Pt (Weller *et al* 1993) and Co/Pd (Engel *et al* 1991a) grown using seeded epitaxy on GaAs substrates (Lee *et al* 1990). Here XRD studies revealed that again little or no strain is present in these MBE prepared layers. Evidence was found for the presence of an ordered $CoPt_3$ phase at the interfaces of Co/Pt multilayers grown at elevated temperatures (Toney *et al* 1992). The percentage of this ordered phase was limited to only around 20% for the multilayer films considered by Weller *et al* (1993). STM images of the final surface of the (111) oriented Co/Pd sample revealed 500 Å diameter flat-topped grains separated by 50 Å wide by 50 Å

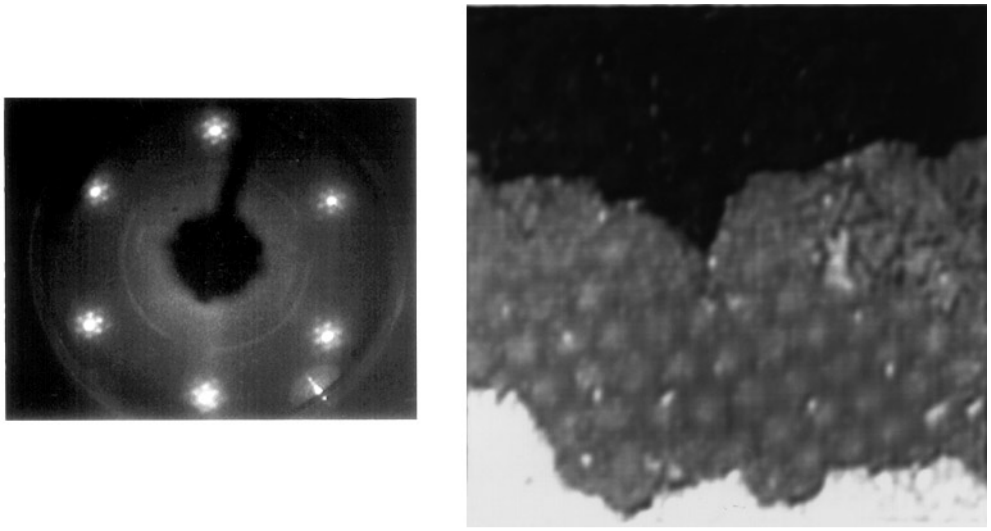

(*a*) (*b*)

Figure 12. (*a*) LEED pattern (Purcell *et al* 1993) and (*b*) STM picture (Kohlhepp and Jungblut unpublished) of about 10 Å of Co on Pd(111), both showing the superstructure due to the in-plane lattice mismatch between Co and Pd. The area displayed in the STM picture measures 40 nm × 40 nm and shows monoatomic Co steps with a clear superstructure on the middle terrace.

deep valleys (Engel *et al* 1991a). In summary, both Co/Pd(111) and Co/Pt(111) grow in an incoherent mode, and exhibit little strain.

In contrast to the relaxed growth in the (111) orientation, den Broeder *et al* (1989) established that (100) oriented Co/Pd multilayers maintained a coherent epitaxial growth up to at least 6 MLs of Co. Although this observation is rather surprising on energetic grounds—the critical thickness for the coherent/incoherent growth transition of such a large lattice mismatch system is around 1 ML, as found for the (111) orientation—it appears to be of general applicability, as both the seeded epitaxial MBE-grown Co/Pt(100) (Weller *et al* 1993) and Co/Pd(100) (Engel *et al* 1991a) multilayers grew coherently in the thickness ranges investigated. In the latter case, a perpendicular contraction of the Co of around 10%, coupled with an in-plane expansion of around 8% was reported (Engel *et al* 1991b). Such coherent growth induces considerable stresses, which will strongly influence the anisotropy properties of both (100) oriented Co/Pt and Co/Pd multilayers. Moreover the Co(100) has a fcc structure. The Co/Pd(100) multilayers were shown by STM to consist of 1000 Å diameter flat grains (Engel *et al* 1991b).

The growth of the (110) oriented Co/Pd and Co/Pt multilayers is less well characterized. The Co lattice in (110) Co/Pt may exhibit an orthorhombic distortion (Le Dang *et al* 1994), whereas the XRD intensity of the (110) Co/Pd samples was insufficient to perform a meaningful analysis of the lattice strain (Engel *et al* 1991b). The surface of the (110) oriented Co/Pd multilayer, as probed by STM, revealed large, flat patches of 4000 Å extent separated by 200 Å deep and 1000 Å wide valleys.

7.1.2. Co/Ni sandwiches grown on single-crystal Cu substrates. To study the orientational dependence of the PMA in the Co/Ni system, three epitaxial Ni/Co wedge/Ni sandwiches

were deposited onto Cu single-crystal substrates of crystallographic orientation (100), (111) and (110) (Johnson *et al* 1992). Co, Ni and Cu have similar lattice constants, which should encourage coherent epitaxial growth for the relatively thin Co and Ni layers investigated. The perpendicular and parallel lattice spacings were determined as a function of Co thickness by performing several LEED measurements along the Co wedge. Both the Co and Ni displayed fcc surface nets which were nearly identical to that of the Cu substrates. Such coherent growth results in an in-plane expansion of the respective lattices by 2% (Co) and 2.5% (Ni), and introduces strains into the growing films. The in-plane lattice expansions were found to be accompanied by perpendicular lattice contractions (Poisson contractions), resulting in perpendicular spacings of 1.71 Å, 1.21 Å and 2.01 Å for the respective (100), (110) and (111) orientations—less than the corresponding Cu–Cu lattice spacing of 1.81 Å, 1.27 Å and 2.09 Å.

7.1.3. Co/Cu and Ni/Cu bilayers on single crystal Cu substrates. Maintaining the lattice distortion associated with the coherent growth requires a considerable amount of elastic energy. Above the critical thickness introduced in subsection 2.3, this energy becomes too great, and relaxation towards the bulk lattice parameters will occur via introduction of misfit dislocations. Co/Cu and Ni/Cu are two systems where the respective lattice mismatch of 2.0% and 2.5% may induce relaxation of coherent epitaxial growth for thicker layers. Such behaviour, together with the associated consequences for the assignment of anisotropies to interface or volume anisotropy, has been discussed in considerable detail for MBE-grown Cu/Ni-wedge/Cu(100) and Cu/Ni-wedge/Cu(111) systems in subsection 6.2 (Jungblut *et al* 1994). For the MBE growth of ultrathin Co/Cu bilayers and wedges on Cu single-crystal substrates of crystallographic orientation (100) and (111), the smaller lattice mismatch of 2.0% maintained a coherent epitaxial growth mode for most samples used for anisotropy studies (de Miguel *et al* 1991, Heinrich *et al* 1991b). The situation for growth on the lower symmetry (110) Cu substrate was somewhat more complicated. Here, LEED studies indicated that the Co growth is initially coherent, with streaking occurring along the [001] direction (the open direction in the (110) surface) as growth proceeds. Although such streaking could be interpreted as the onset of partially incoherent growth, recent STM observations suggest that a more likely explanation is the presence of elongated islands growing in the [110] directions (Kohlhepp *et al* unpublished). For all MBE-grown Co/Cu and Ni/Cu samples, it is therefore possible to identify at least an initial range of magnetic layer thickness where coherent epitaxial growth occurs, and in which the pure Néel interface anisotropy may be determined.

7.2. Interfacial and volume anisotropy

In table 7, results are accumulated of the orientational dependence of both interface and volume anisotropy contributions for several Co- and Ni-based multilayer systems. Here, the volume anisotropy contribution includes the demagnetization term ($-\frac{1}{2}\mu_o M_s^2$ for a thin film).

7.2.1. Co/Pt. In figure 13, the orientational dependence of the anisotropy of the MBE-grown Co/Pt multilayers is presented in the usual fashion (Weller *et al* 1993). Extrapolation of the linear sections of this figure yields the interface anisotropy; the slope reflects the volume contribution to the total anisotropy. Perpendicularly oriented multilayers have positive anisotropy. The results are compiled in table 7. It is clear that each of the multilayer orientations has different interface and volume anisotropy contributions. The

Table 7. Orientational dependence of the interface (K_s) and volume (K_v) anisotropy contributions in MBE-grown Co- and Ni-based multilayers. Theoretical predictions of K_s and K_v and associated references are shown in parentheses. Calculations determine only anisotropy energies for given multilayer structures; separation into K_s and K_v is somewhat arbitrary.

Sample	Orientation	K_s (mJ m^{-2})	K_v (MJ m^{-3})	Reference
Co/Pt	(111)	0.97 (0.85)	−0.74 (−1.3)	Weller *et al* (1993)
	(110)	0.42 (0.7)[a]	−1.95 (−4.2)[a]	(Victora and
	(100)	0.59 (0.6)[a]	−5.98 (−6.4)[a]	MacLaren 1993a)
Co/Pt (bilayer)	(111)	1.15 (0.85)	−0.77 (−1.3)	McGee *et al* (1993)
Co/Pd	(111)	0.63 (0.66)	−0.5 (−1.8)	Engel *et al* (1991a)
	(110)	0.63	−1.82	(Victora and
	(100)	0.63 (0.57)	−4.5 (−6.4)	MacLaren 1993b)
Co/Pd (bilayer)	(111)	0.92 (1.1)[b]	−1.0	Purcell *et al* (1993) (Daalderop *et al* 1990b, 1991)
Co/Ni	(111)	0.42 (0.5)[b]		Johnson *et al* (1992)
	(110)	0.19		
	(100)	0.23		(Daalderop *et al* 1992)
Co/Cu	(111)	0.21	−0.9	Hillebrands *et al* (1994),
	(110)	−0.86	Various	Fassbender *et al* (1995)
	(100)	0.15	−1.2	
Ni/Cu[c]	(111)	−0.08	0.13	Jungblut *et al* (1994)
	(100)	−0.4	0.39	

[a] Extrapolated from Co_1/Pt_5 *ab initio* calculation, assuming analogous orientational behaviour in Co/Pt and Co/Pd.
[b] Extrapolated from calculated $K_{eff}t_{Co}$ at 2 Å Co, using experimental K_v.
[c] Measurements in the coherent epitaxial growth region: $t_{Ni} < 32$ Å (111); < 42 Å (100).

strongest perpendicular anisotropy at all Co thicknesses is present in the (111) orientation, where K_s is maximum (0.97 mJ m^{-2}) and, reflecting the low stress of the incoherent (111) growth, K_v minimum (−0.74 MJ m^{-3}). The value of K_s for the (111) multilayers is somewhat smaller than that of a Co/Pt bilayer grown on a single crystalline Pt(111) substrate ($K_s = 1.15$ mJ m^{-2}), whereas K_v is rather similar (McGee *et al* 1993). The (100) multilayers displayed an extremely large negative volume anisotropy, in line with the large coherency strain in these layers and the positive magnetostriction. With such a large volume anisotropy, extrapolation of the steeply sloping line to define K_s with the associated reliance on data points at small Co layer thicknesses introduces some uncertainty in the values of K_s: the extrapolated value of 0.59 mJ m^{-2} is however significantly different from that of the (111) orientation. The (110) oriented multilayers displayed a still lower interface anisotropy: 0.42 mJ m^{-2}, and a volume anisotropy contribution intermediate between that of the (100) and (111) orientations.

7.2.2. Co/Pd. In almost all systems presented in table 7, a strong orientational dependence of K_s and K_v is observed, and also predicted from the *ab initio* theory. An exception is formed by the Co/Pd system, where an orientation-independent K_s was determined for

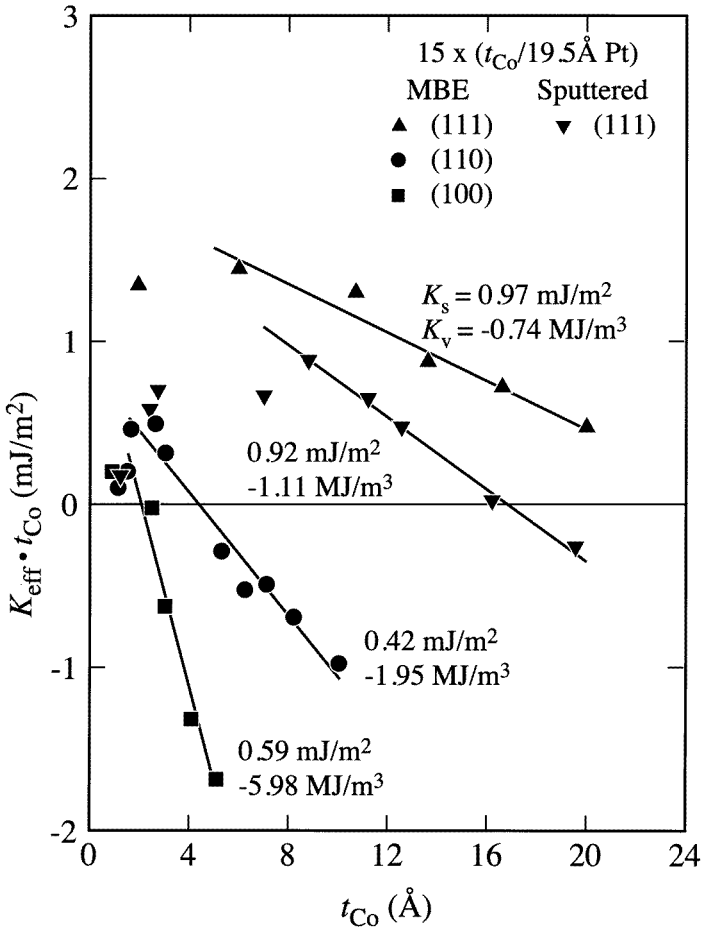

Figure 13. Orientational dependence of the volume and interface anisotropy contributions in seeded epitaxial-grown Co/Pt multilayers, after Weller *et al* (1993).

three series of thick multilayers prepared by seeded epitaxy techniques (Engel *et al* 1991a). Due to the similarities in growth of Co/Pd and Co/Pt, the volume anisotropy contribution of the Co/Pd multilayers followed an identical trend to that discussed above for the Co/Pt multilayers. Despite the wide variation in the volume anisotropy contribution, the interface anisotropy was 0.63 mJ m^{-2} for all Co/Pd orientations (see figure 14). Although explained theoretically by a fortuitous consequence of the precise degree of strain exhibited by the Co/Pd system (Victora and MacLaren 1993b), it may also here be questioned whether K_s is truly orientation independent: in at least the (111) orientation a considerably higher value of K_s has been reported for a Co/Pd bilayer grown directly onto a Pd(111) single crystal (Purcell *et al* 1993). This bilayer sample also had a significantly different volume anisotropy as that of the (111) oriented multilayer, namely -1.0 MJ m^{-3}. The difference between this value and the shape anisotropy (-1.27 MJ m^{-3}) could result from the presence of hcp Co regions—the magnetocrystalline anisotropy of bulk Co equals 0.53 (Landolt-Börnstein 1986). In contrast, for the (111) oriented Co/Pd multilayer $K_v = -0.5$ MJ m^{-3}, the difference of 0.77 MJ m^{-3} with the shape anisotropy exceeds the magnetocrystalline

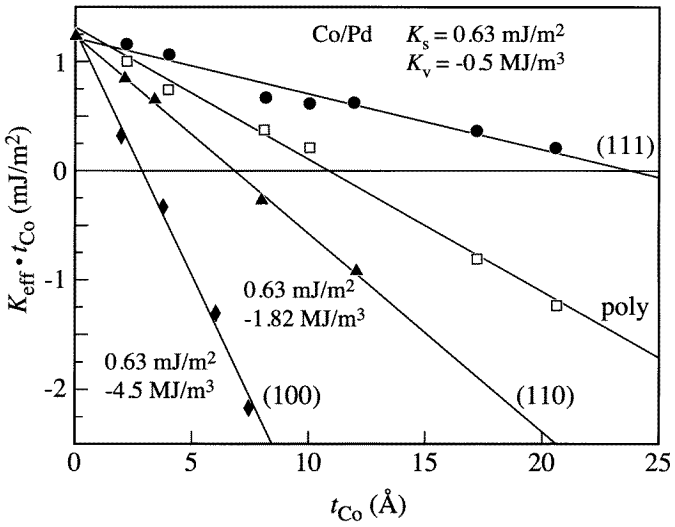

Figure 14. Orientational dependence of the volume and interface anisotropy contributions in seeded epitaxial-grown Co/Pd multilayers, after Engel *et al* (1991a).

anisotropy of Co. Additional factors must be contributing: a small residual in-plane tensile strain (0.2%), a reduction in M_s due to interface diffusion or alloying or a reduction in the shape anisotropy of the thicker multilayer as a result of the pronounced columnar structure revealed by STM are all candidates. A magneto-elastic anisotropy contribution was sufficient to account for the large negative K_v of the (100) oriented Co/Pd multilayer. Using the measured lattice strain and assuming a magnetostriction constant $\lambda_{100} = 130 \times 10^{-6}$—for Co-rich fcc CoPd alloys (Tokunaga *et al* 1981)—an additional magneto-elastic anisotropy contribution of -2.8 MJ m^{-3} was calculated, close to the experimentally determined K_v (excluding shape anisotropy) of -3.2 MJ m^{-3}. In the previous section, attention was paid to those aspects which, even in MBE-prepared samples, may influence quantitative comparison between measured and calculated PMA.

7.2.3. Co/Ni. The discovery of PMA in Co/Ni is of particular interest, as both the multilayer components are magnetic (Daalderop *et al* 1992). The orientational dependence of the magnetic anisotropy of Co/Ni was determined by MOKE measurements at various positions along three separate Co wedges, one sample for each of the three primary orientations (100), (110) and (111), prepared on single-crystalline Cu substrates. As each sample consists of a Cu/Ni/Co wedge/Ni/Cu layering, an effective 'interface' anisotropy ($K_{s,eff}$) must now be defined, comprising the interface anisotropies of Co/Ni (two interfaces), Cu/Ni (two interfaces) and the volume anisotropy of a fixed thickness of Ni (Johnson *et al* 1992).

In figure 15(*c*), it is seen that the (111)-oriented sample displays PMA for all Co thicknesses investigated, with an effective total interface anisotropy. Subtracting the volume contribution of the Ni and the Cu/Ni interface contribution (measured total value: 0.14 mJ m^{-2}), one obtains $K_s^{Co/Ni(111)} = 0.42$ mJ m^{-2}, i.e. an interface contribution favouring PMA. The importance of the interface in enhancing the perpendicular anisotropy is emphasized in the region below $t_{Co} = 2$ Å. On average the Co thickness in this region is less than one monolayer, so that the film will consist of isolated Co patches; between these

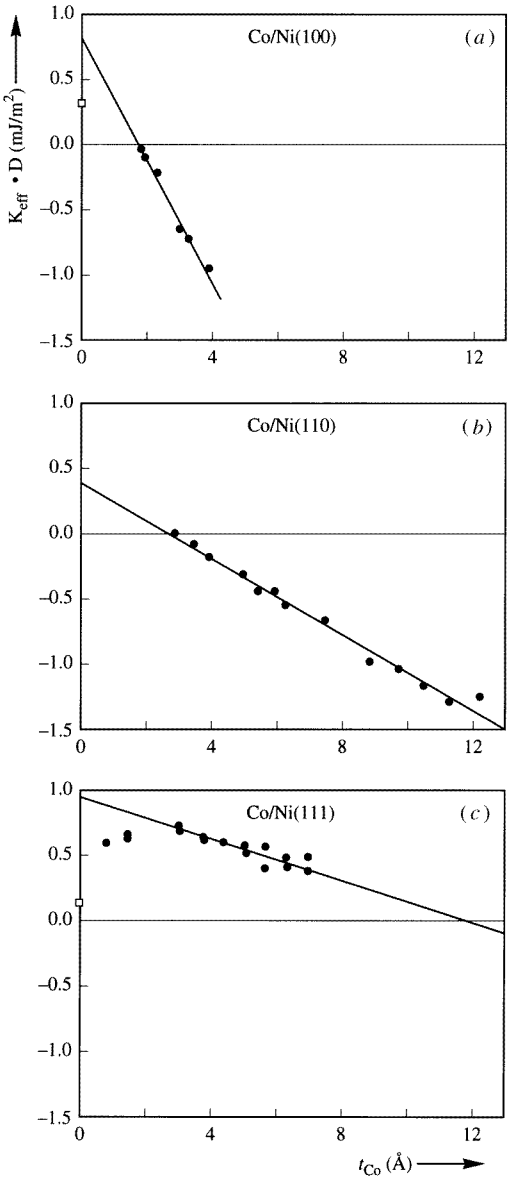

Figure 15. Orientational dependence of the volume and interface anisotropy contributions in Ni/Co/Ni sandwiches epitaxially grown on single-crystal Cu substrates, after Johnson *et al* (1992). The product of total anisotropy $K_{\rm eff}$ and total magnetic layer thickness D, plotted as a function of Co thickness for the (*a*) (100), (*b*) (110) and (*c*) (111) orientation. Each single data point at $t_{\rm Co} = 0$ Å (open square) yields the sum of the Ni volume and Cu/Ni interface contribution to the anisotropy.

patches, the Ni overlayer will grow directly onto the Ni underlayer, and no Co/Ni interface will form, so that the PMA is reduced. This explains the observed deviation from linear behaviour below 2 Å in figure 15(*c*).

Similar analysis of figure 15(*a*) for the (100) sample yields $2K_{\rm s,eff} = 0.78$ mJ m^{-2}. The reference measurement before the start of the Co wedge produced a value of 0.32 mJ m^{-2} for the sum of the Ni volume and Cu/Ni interface contributions, thus yielding $K_{\rm s}^{\rm Co/Ni(100)} = 0.23$ mJ m^{-2}.

In the case of the (110) orientation, figure 15(*b*) reveals a vertical intercept $2K_{\rm s,eff} = 0.38$ mJ m^{-2}. Reference measurements before the start of the wedge were unable to quantify the Ni and Cu/Ni interface contributions, although these were always positive. It is thus

concluded that at most $K_s^{Co/Ni} < 0.19$ mJ m^{-2}. This is sufficient to show that the three samples demonstrate different interface anisotropy contributions, as summarized in table 7. As the growth of the Co/Ni sample on the Cu single crystal is coherent epitaxial, the Co volume anisotropy contributions reported in (Johnson *et al* 1992) are at least partly attributed to a magneto-elastic anisotropy, induced by the mismatch with the Cu substrate, and are not representative of Co/Ni multilayers. For this reason, an orientational dependence of K_v is not included in table 7.

7.2.4. Co/Cu and Ni/Cu. The Co/Cu and Ni/Cu systems do not exhibit large perpendicular magnetic anisotropies, primarily due to the absence of a strong positive K_s which would induce a perpendicular alignment of the magnetization. This reluctance to exhibit a perpendicular magnetization over a wide range of magnetic layer thickness makes these systems less suitable for magneto-optical or magnetic storage applications than Co/Pt, Co/Pd or Co/Ni; as a consequence the PMA in Co/Cu and Ni/Cu has been less extensively studied.

For (111)-oriented Co/Cu Lee *et al* (1990) explained the thickness dependence of the anisotropy of MBE-grown multilayers as being due solely to a Co-layer misfit strain variation, i.e. K_s was taken to be zero. More recent studies by Hillebrands *et al* (1994) on a Cu(111)/Co wedge/Cu sandwich did, however, reveal a weak interface anisotropy contribution of $K_s^{Co/Cu(111)} = 0.21$ mJ m^{-2} (MOKE measurements) or 0.13 mJ m^{-2} (BLS measurements). An associated volume anisotropy contribution of around -0.9 MJ m^{-3} was determined by both techniques. Additional measurements by Kohlhepp *et al* (1992) and den Broeder *et al* (1991) confirmed that the Co/Cu(111) system indeed displays a weak perpendicular interface anisotropy of 0.1–0.2 mJ m^{-2}. Due to the large negative volume anisotropy, perpendicular magnetic anisotropy was limited to below 3 Å Co. The anisotropy of Co/Cu(100) has been extensively discussed by Heinrich *et al* (1991b) and Krams *et al* (1992). Once again, a rather weak interface anisotropy contribution was identified after accounting for the in-plane anisotropy terms, values of $K_s^{Co/Cu(100)} = 0.15$ mJ m^{-2} and $K_v = -1.2$ MJ m^{-3} are in fact rather similar to that of the (111) orientation. The Co thickness dependence of the anisotropy of (110) oriented Co/Cu behaved differently to either the (111) or (100) orientation, with a strong, in-plane interface contribution being identified ($K_s^{Co/Cu(110)} = -0.89$ mJ m^{-2}). The anisotropy behaved in a complicated manner at larger thicknesses, suggesting either considerable variations in either the magneto-elastic anisotropy, or perhaps changes in the shape anisotropy associated with the characteristic growth mode of the (110) system (elongated islands). A detailed analysis of the anisotropy is given by Hillebrands *et al* (1996).

The details of the Ni-thickness dependence of the magnetic anisotropy of (100)- and (111)-oriented MBE-grown Cu/Ni sandwiches have been discussed in considerable detail in subsection 6.2 (Jungblut *et al* 1994). Although both the volume and interface anisotropy contributions were influenced by the details of the magneto-elastic anisotropy, it was possible to define a value for K_s, of electronic origin. The orientationally dependent interface anisotropy contributions shown in table 7, $K_s^{Ni/Cu(111)} = -0.08$ mJ m^{-2} and $K_s^{Ni/Cu(100)} = -0.40$ mJ m^{-2}, (weakly) favour in-plane magnetization.

7.3. Theoretical predictions of PMA

The magnetic anisotropy energy is a relatively small energy term in an *ab initio* calculation. Pioneering work by Gay and Richter (1987a) on the calculation of magnetic anisotropy energy in free standing magnetic monolayers, was later extended to a series of first-principles

calculations on Co-based multilayers (Daalderop *et al* 1990b, 1991, 1992, 1994, Victora and MacLaren 1993a, b, Kyuno *et al* 1992). In these calculations, the magnetic anisotropy is of the order of 1 meV/Co atom and can be related to the spin–orbit interaction induced splitting and shifting of electronic states which depend on the magnetization direction (Daalderop *et al* 1994). As such, only those systems with relatively large PMA (Co/Pt, Co/Pd, Co/Ni) have been extensively investigated from the theoretical point of view. The theoretical predictions of PMA are also presented, in parentheses, in table 7. It should be noted that each calculation determines only the total magnetic anisotropy energy for a given multilayer structure. As a consequence, the separation of this anisotropy into a volume and interface contribution is somewhat arbitrary.

7.3.1. Co/Ni. With its coherent epitaxial growth in all three orientational directions, the Co/Ni system is well suited to theoretical investigations with their inherent pseudomorphic structures. Such a theoretical study was undertaken prior to any experimental investigation (Daalderop *et al* 1992). In the Co/Ni(111) system, the precise location of the Fermi level played an important role in determining the magnitude of the PMA. This effect is seen most strikingly in the difference between the anisotropy energies of Co_1/Ni_2 and Co_2/Ni_1 multilayers (the subscripts denote the number of monolayers) where a rigid-band behaviour is found (Daalderop *et al* 1992), see figure 16. Co_1/Ni_2 has a strong PMA whilst Co_2/Ni_1 was predicted to be in-plane. Co_1/Ni_5 proved an intermediate case, at the transition between in-plane and perpendicular magnetization. Such differences could not be accounted for by differences in shape anisotropy (not included in figure 16), or the magneto-elastic

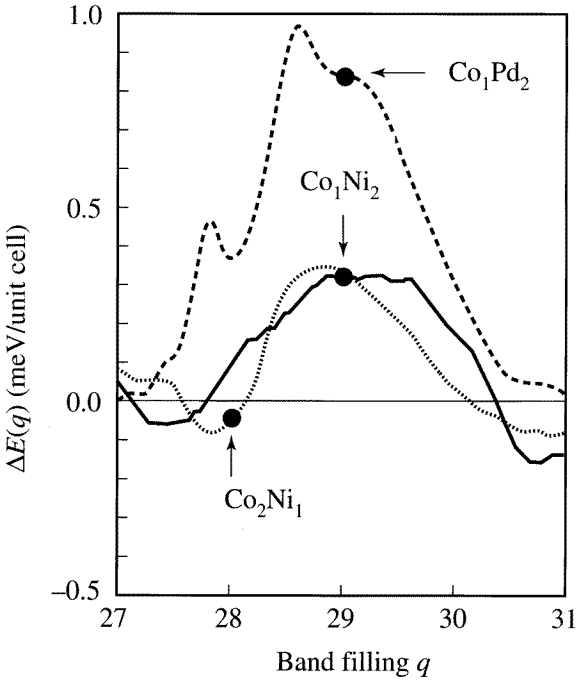

Figure 16. MAE as a function of band filling calculated using the self-consistent band structure of Co_1/Ni_2 (full curve, $n = 29$), Co_1/Pd_2 (broken curve, $n = 29$) and Co_2/Ni_1 (dotted curve, $n = 28$). The demagnetization energy is not included. After Daalderop *et al* (1992).

anisotropy of the coherently grown Co/Ni system (small in magnitude, favouring in-plane magnetization). The sensitivity of the magnetic anisotropy of Co/Ni and Co/Pd to band filling (figure 16) emphasizes the role played by the interface electronic structure. An analysis of various contributions to the anisotropy energy allowed the assignment of PMA in Co_1/Ni_2 (and other Co_1/X_2 multilayers) to the spin–orbit interaction of states with $d_{x^2-y^2}$ and d_{xy} character present close to the Fermi level. Calculations of the magnetic anisotropy of Co/Ni for other orientations have not yet been attempted. However, as in Néel's (1954) model, the itinerant-electron model also leads naturally to the prediction of orientationally dependent interface anisotropies: by breaking the crystal symmetry in different orientations, the splitting of degenerate states by the spin–orbit coupling will be more or less effective. For example, it has been shown that the lifting of two-fold degeneracies plays an important role in determining the PMA of (111) oriented multilayers (Daalderop *et al* 1994). It is, therefore, anticipated that lower symmetry interfaces, such as (110), which has no degeneracies, will exhibit a very different interface anisotropy. As such, an orientation-dependent anisotropy would be anticipated in Co/Ni.

7.3.2. Co/Pd. Two approaches have been taken to the calculation of the magnetic anisotropy energy in Co/Pd multilayers. A first-principles spin-polarized calculation for (100)- and (111)-oriented Co/Pd structures was carried out by Daalderop and co-workers (1990a, b, 1991, 1994), whereas Victora and MacLaren (1993b) performed calculations for the same orientations using the layered KKR method. Globally, the two approaches generated rather similar results (see figure 17), although extrapolation of the calculations to separate the total anisotropy energy into a volume and interface contribution resulted in an appreciable difference in K_s for the (111) orientation: $K_s^{Co/Pd(111)} = 1.1$ mJ m^{-2} (Daalderop *et al* 1990b, 1991), $K_s^{Co/Pd(111)} = 0.66$ mJ m^{-2} (Victora and MacLaren 1993b). Although the KKR method resulted in an orientation-independent K_s (see table 7), the differences in anisotropies calculated by the two methods, and the orientational dependence noted in the spin-polarized calculations, suggest that this may not be the case. This point will be discussed in some detail below.

7.3.3. Co/Pt. Victora and MacLaren applied their layer KKR method, developed for the Co/Pd system, to Co/Pt (Victora and MacLaren 1993a). Arguing that Pt and Pd have similar lattice constants, they assumed that the Co–Co interaction constants deduced from the Co/Pd calculations may remain valid for the Co/Pt system. Only the Co–Pt interaction constant in the (111) orientation was calculated, the remaining anisotropies were inferred by assuming a similar orientational dependence of the strain in Co/Pt as in Co/Pd. The results are reported in table 7. A first-principles approach to calculate the anisotropy in Co/Pt multilayers was undertaken by Daalderop *et al* (1990b, 1991, 1994). Convergence of the calculations was, however, poor, leading to substantial differences between the values calculated for Co_1/Pt_2 and Co_1/Pt_5. Investigating the variation of the magnetic anisotropy of Co/Pt with band filling, a similar behaviour to that of Co/Pd in figure 16 was found, shifted, however, such that Co_1/Pt_2 falls on the steeply rising flank. For this reason, the anisotropy was very sensitive to details of the calculation (number of Pt layers, spd or $spdf$ band basis) and a reliable anisotropy energy was not reported.

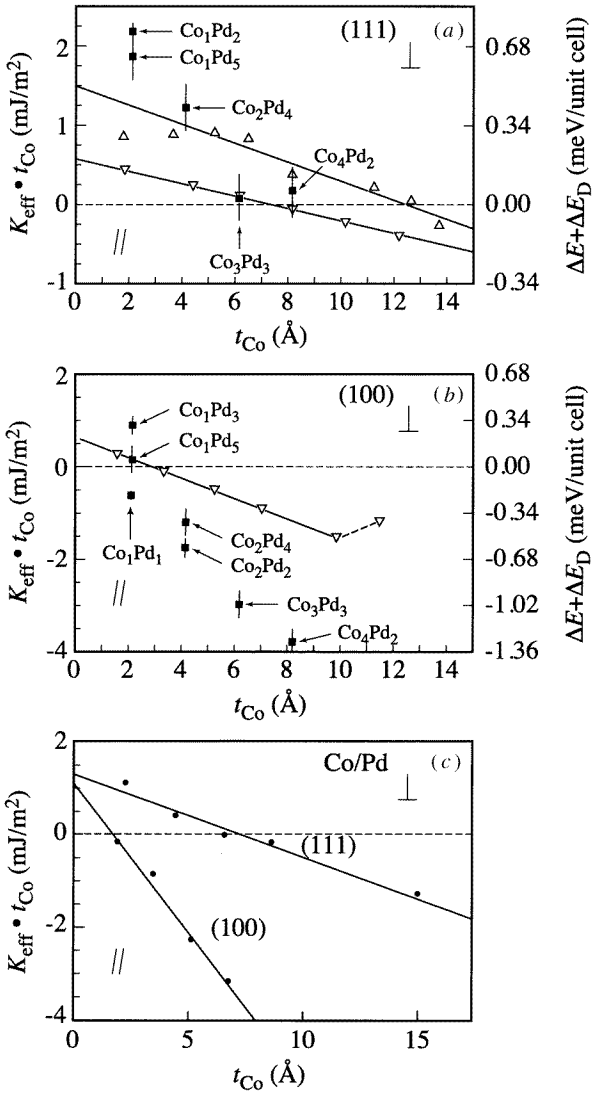

Figure 17. MAE times Co thickness versus Co thickness in the Co/Pd system. (*a*) (111) orientation from spin-polarized band-structure calculations by Daalderop *et al* (1990b), (*b*) (100) orientation from spin-polarized band-structure calculations by Daalderop *et al* (1991), (*c*) (100) and (111) orientation using layer KKR method by Victora and MacLaren (1993b).

7.4. Comparing measured and calculated PMA

When can a meaningful comparison between measured and calculated anisotropies be made? Perhaps the major uncertainty associated with the *ab initio* calculations is the necessity to use a structural model with the lattices of adjacent metal layers in full registry with each other (coherent epitaxial model) for systems such as Co/Pd and Co/Pt, where lattice misfits in the order of 10% quickly lead to incoherent (relaxed) growth. More success may be anticipated for lower mismatch, coherently grown systems, such as Co/Ni (mismatch 0.6%), where theoretical predictions were the driving force behind the subsequent experimental

determination of a PMA (Daalderop *et al* 1992).

There is certainly room to improve the calculations which, so far, all make use of some form of shape approximation (muffin-tin potential or atomic-spheres approximation) and are based on a frozen potential approximation. The orbital polarization term which yields enhanced values of L_z, as confirmed by magnetic circular x-ray dichroism (MCXD) experiments (Weller *et al* 1994), also leads to larger values of the magnetic anisotropy energy. In a number of cases (Daalderop *et al* 1990b, 1991) this leads to results which are in better agreement with experiment. For the artificial multilayers, however, this means that calculated anisotropy energies which already exceed the experimental values become even larger.

This could be understood if experiments were consistently underestimating interface anisotropies, so that caution should also be exercised in interpreting the measurement of PMA. Recently, several factors have been established to modify in particular the measured value of K_s, in general leading to a reduction of PMA. For example, roughness and the formation (by interdiffusion) of interface alloys are seen to influence K_s and are particularly important in sputtered samples (subsection 6.1). In sputtered Co/Pd multilayers, Nakamura *et al* (1991) considered that PMA is caused mainly by interfacial strain anisotropy of the interface alloy. Roughness in general reduces the magnitude of K_s, as supported by the systematic increase of K_s for a variety of systems prepared by MBE compared to sputtered samples, compare e.g. Daalderop *et al* (1992) and Johnson *et al* (1992). The influence of microscopic roughness, as predicted by Bruno (1988b), has been quantified in an elegant series of experiments on Fe/Au multilayers (Robl 1993). When thicker (multi-)layers are prepared in particular using evaporation techniques, geometrical self-shadowing effects tend to induce columnar growth and curved layers (Bales and Zangwill 1991, de Veirman *et al* 1992). The consequence may be a 'macroscopic' granularity which may reduce the effective area of the interface. Such behaviour may account for the reduction of K_s in the thicker Co/Pd(111) multilayers, where STM measurements revealed 500 Å diameter columns separated by 50 Å wide and deep valleys (Engel *et al* 1991a), compared with K_s measured for a thin Co/Pd bilayer deposited directly onto a Pd(111) single crystal, where the majority of the interface area should contribute to K_s (Purcell *et al* 1993). The contribution of the effective interface area to the measured PMA is further illustrated for ultrathin (sub-)monolayers. For Co/Ni(111) for example, a clear reduction in PMA below a Co thickness of 2 Å (1 ML) attests to the reduction in interface area contributing to the PMA as the Co layer breaks up into patches, see figure 15 (Johnson *et al* 1992). In most cases (other than for some possible interface alloys), the experimental artefacts mentioned above will result in a reduction of K_s from its intrinsic value (that of a perfectly flat interface). As calculations are more closely akin to the situation of the perfect interface, it is to be expected that theoretical predictions should mostly exceed the experimentally determined values. That this is not always the case (see Co/Pt, Co/Pd systems in table 7) may be reconciled with the difficulty in creating realistic calculations for incoherent or partially strained systems.

Taking these factors into account, it is perhaps reasonable to consider the coherent epitaxial MBE grown Co/Ni as the system most suitable to test the theoretical investigations. For (111) Co/Ni, a hypothetical Co_1/Ni_2 cell was predicted to display an anisotropy of $KD = 0.65 \pm 0.10$ mJ m^{-2} (with D the bilayer period) (Daalderop *et al* 1992), whereas application of the K_s value for Co/Ni(111) from table 7 to the same Co_1/Ni_2 cell yielded $KD = 0.53$ mJ m^{-2} after compensating for shape anisotropy (Johnson *et al* 1992). Extrapolation of the theoretical anisotropy of the Co_1/Ni_2 cell using the experimentally determined volume anisotropy resulted in a close agreement between experimental ($K_s =$

0.42 mJ m^{-2}) and theoretical ($K_s = 0.5$ mJ m^{-2}) interface anisotropy contributions. The agreement between theory and experiment is more striking in that the theoretical prediction was made before the experimental investigation was undertaken.

For the seeded epitaxial Co/Pt multilayers, inspection of table 7 shows that the theory of Victora and MacLaren (1993a) gives good agreement for both K_s and K_v (controlled by coherency strains) for the (100) oriented multilayers, but poor agreement for the other orientations (Weller *et al* 1993). In particular, the theory predicts a value of K_s which is too small for the (111)-oriented multilayers, and especially for the Pt/Co wedge/Pt(111) sample of McGee *et al* (1993). Such behaviour may be anticipated, as only the (100) multilayers exhibit the pseudomorphic growth mode required by the model calculations. To obtain a better description of the experimental situation, it is suggested that the model should in future incorporate the effects of alloying, chemical ordering ($CoPt_3$ phases) and Pt polarization.

In contrast to all other multilayer series in table 7, the interface anisotropy of the Co/Pd multilayers was observed to be orientationally independent (Engel *et al* 1991a), with a magnitude of around 0.6 mJ m^{-2}. The theoretical K_s values were found to be remarkably similar, and thus also almost independent of orientation. The experimental K_s in the (100) orientation, however, exceeds the experimental value, which would not be anticipated from the observed growth imperfections. Although explained theoretically by a fortuitous consequence of the precise degree of strain exhibited by the Co/Pd system (Victora and MacLaren 1993b), it may also here be questioned whether K_s is truly orientation independent. In at least the (111) orientation a considerably higher experimental value of K_s has been reported: $K_s^{Co/Pd(111)} = 0.92$ mJ m^{-2} (Purcell *et al* 1993). For Co/Pd, the (111) orientation exhibits direct incoherent epitaxial growth, and therefore calculations may be less reliable. Despite this, Daalderop and co-workers have calculated the magnetic anisotropy for a hypothetical Co_1/Pd_2 cell. Here, an anisotropy of $KD = 1.85 \pm 0.25$ mJ m^{-2} was predicted (Daalderop *et al* 1990b, 1991). Application of the K_s value for Co/Pd bilayer grown on a Pd(111) single crystal (from table 7) to this Co_1/Pd_2 cell yielded $KD = 1.6$ mJ m^{-2} after compensating for shape anisotropy (Johnson *et al* 1992). Extrapolation of the theoretical anisotropy of the Co_1/Pd_2 cell using the experimentally determined volume anisotropy resulted in a close agreement between experimental ($K_s = 0.92$ mJ m^{-2}) and theoretical ($K_s = 1.1$ mJ m^{-2}) interface anisotropy contributions. The theoretical K_s of Daalderop *et al* (1990b, 1991) exceeds the measured value, as generally expected from the above considerations. The same authors also calculated the magnetic anisotropy for hypothetical (100) oriented Co_1/Pd_3 and Co_1/Pd_5 cells. The predicted anisotropy was $KD = 0.6 \pm 0.3$ mJ m^{-2} in these cases (Daalderop *et al* 1994), significantly lower than in the (111) orientation, but similar to the experimental findings (Engel *et al* 1991a). Due to the large volume anisotropy, and difference between the Co_1/Pd_3 and Co_1/Pd_5 anisotropies, an extrapolation to K_s was considered inappropriate. It appears, however, that also from the theoretical viewpoint the interface anisotropy in Co/Pd may be orientation dependent.

8. Surface versus interface anisotropy

The distinction between surface and interface is based on the presence, at the boundary of a material, of either vacuum or another material. Theoretically, the magnetic anisotropy of a free-standing Co monolayer, hence with two *surfaces*, has been calculated and resulted in an in-plane easy axis (Gay and Richter 1987a, b, Bruno 1989). Such a free standing monolayer cannot be realized experimentally as some means of support is required. One

Table 8. Table of out-of-plane surface anisotropies per surface. Positive values support a perpendicular easy axis.

Surface	K_s (mJ m^{-2})	Reference
Fe(100)/UHV	0.96	Heinrich *et al* (1991a), Cochran *et al* (1988)
Fe(110)/UHV	0.97	Fritzsche *et al* (1994), Elmers and Gradmann (1990)
Co(111)/UHV	−0.28	Ould-Mahfoud *et al* (1993)
Co(111)/UHV	−0.17	Beauvillain *et al* (1994)
Co(100)/UHV	−1.06	Krams *et al* (1992)
Co(0001)/UHV	−0.28	Kohlhepp and Gradmann (1995)
Ni(111)/UHV	−0.48	Gradmann *et al* (1984)

surface can be made, however, although only a few research groups are equipped for *in situ* (to avoid contamination) characterization of the magnetic anisotropy.

The surface anisotropy is usually obtained in a study of the dependence of the magnetic anisotropy on the thickness of a non-magnetic overlayer. After subtracting the contribution of the interface with the supporting substrate found in the same study—often the substrate is made of the same material as the overlayer—or obtained from the literature, the contribution of the surface remains. In this way the values in table 8 were obtained. A very large contribution was found by Krams *et al* (1992) $K_s^{\mathrm{Co/UHV(100)}} = -1.06 \pm 0.17$ mJ m^{-2}. The most detailed study is that by Kohlhepp and Gradmann (1995) of Pd/Co(0001) with Pd and Ag overlayers, where not only a second order anisotropy constant $K_{s,2}^{\mathrm{Co(0001)/UHV}} = -0.28$ mJ m^{-2} but also a fourth-order anisotropy constant $K_{s,4}^{\mathrm{Co(0001)/UHV}} = -0.09$ mJ m^{-2} was obtained. In these studies some assumptions had to be made, e.g. in the sandwiches both interfaces have the same K_s and the first interface keeps the same K_s for any coverage. Theoretical predictions have only addressed the effective (volume and surface) anisotropies of free standing monolayers and favour mainly an in-plane easy axis (Daalderop *et al* 1994, Bruno 1989).

Further, in the study of the anisotropy as a function of the overlayer thickness a remarkable observation is made. Although sometimes a gradual dependence on the overlayer thickness appears (Gradmann *et al* 1984, Bergter *et al* 1985), often a peak around 1 ML coverage is observed in the anisotropy (Engel *et al* 1993a, Wiedmann *et al* 1993, Kohlhepp and Gradmann 1995) or in the related coercive field (Engel *et al* 1993b, c, Ould-Mahfoud *et al* 1993, Beauvillain *et al* 1994). No structural changes are observed in the RHEED analysis that can be related to the observed peak, nor can magneto-elastic contributions account for it since large and small misfit material combinations behave similarly. Therefore the origin is expected to be electronic, which may be indicated by photoemission studies on Co films as a function of Cu coverage (Hartmann *et al* 1993, Ortega *et al* 1993). The electronic origin of this anisotropy peak has since been theoretically confirmed (Újfalussy *et al* 1996).

9. Step anisotropies

In this section the subject of magnetic anisotropies arising from steps will be addressed briefly. It is clear that in practice magnetic films are never perfectly flat but exhibit fluctuations in the layer thickness (steps) resulting from the particular growth mode or from the surface topology of the substrate on which the film has been deposited. Atoms

located at such steps are obviously in a different environment than those located at the flat portions of the surface or within the interior of the film. They are therefore expected to give rise to an additional contribution to the magnetic anisotropy. A quantitative determination of the latter therefore requires control and knowledge of the number of step atoms in the film. One convenient way to manipulate the number of step atoms is to deliberately polish the substrate at a non-zero angle with respect to a crystal axis. Such a procedure yields a terraced surface with known terrace widths and consequently a known number of steps per unit length.

Several experiments employing this technique have been performed (Chen and Erskine 1992, Krams *et al* 1993 and Oepen *et al* 1993). Chen and Erskine (1992) studied ultrathin epitaxial Fe films grown on W(100) surfaces. Using the longitudinal MOKE they found isotropic behaviour for the smooth and two-fold (uniaxial) anisotropic behaviour for the stepped films. The easy in-plane magnetization direction, however, appeared to lie *perpendicular* to the steps, i.e. contrary to what one expects from the shape anisotropy contribution associated with the step geometry. However, a quantitative determination of the step anisotropy was not performed. Berger *et al* (1992), Oepen *et al* (1993) and Krams *et al* (1993) have studied ultrathin epitaxial Co films grown on Cu(1 1 13) surfaces. From angle-dependent MOKE and BLS experiments they also concluded an in-plane uniaxial anisotropy with an easy axis, in this case, parallel to the step edges. From the BLS experiments (Krams *et al* 1993) the uniaxial contribution could be quantified. However, a separation between volume and interface contributions could not be made. For 8 and 12 Å thick films they obtained a value of $(4.4 \pm 0.4) \times 10^4$ J m^{-3}. It is argued that this contribution may be magneto-elastic in origin which according to calculation would yield indeed a comparable value 3.4×10^4 J m^{-3} (Krams *et al* 1993). Furthermore, a switching of the easy axis by 90° upon absorption of submonolayers of Cu, Ag, Fe and O has been observed (Weber *et al* 1995).

Albrecht *et al* (1992) have investigated Fe on W(110). Stepped and smooth surfaces were obtained in their case by using different preparation temperatures. Detailed thickness-dependent studies using TOM and magnetization techniques were performed which allowed for a separation between volume and interface terms. Both in-plane as well as out-of-plane step anisotropies were determined. The results, when corrected for the shape anisotropy contribution which they calculated within the continuous medium approximation, appeared in good agreement with an extension of Néel's model. The agreement concerned the sign and the magnitude as well as the relative magnitudes for the in- and out-of-plane terms.

An interpretation of this step anisotropy in terms of the Néel model is given by Chuang *et al* (1994). Their model properly accounts for the observed behaviour.

10. Summary and concluding remarks

In this review a discussion has been given of the important contributions to the anisotropy of magnetic thin films, such as the magnetic dipolar, the magnetocrystalline and the magnetostrictive contributions. Of particular importance appeared a contribution scaling with the reciprocal magnetic-film thickness: a so-called interface anisotropy. Experimental anisotropy data available from literature at present were commented on. The many experiments have made it clear that interface anisotropies generally exist at all interfaces irrespective of the elements forming the interface. As demonstrated by the Co/Ni multilayer system, for example, they are not restricted to magnetic/non-magnetic interfaces—a finding which is consistent with the general belief that the interface anisotropy basically originates from the lack of translational symmetry at the interface. The experiments have also shown

that the magnetic-interface anisotropies can be several orders of magnitude larger than the magnetocrystalline anisotropies found in bulk crystals and can easily induce perpendicular preferential orientations. An important observation regarding the numerical values is the significant scatter. This makes comparison with theory and the search for trends rather difficult. Most of the scatter is believed to originate from differences in the structure of the layers which is often not well known. For future research, it is therefore important to perform magnetic as well as structural investigations on the same samples. A recent promising experimental development in this respect, is the use of MBE-grown wedge-shaped magnetic layers in combination with (*in situ*) local probes such as MOKE, LEED, RHEED and STM allowing a thickness-dependent study of magnetic and structural properties on one, single, relatively simple and ideal system (only one magnetic layer on a well-prepared single crystal substrate). Apart from the considerable saving of time and effort, accompanied with the preparation of single crystals and the structural investigations, several uncertainties which are commonly present in most studies, are removed, such as varying preparation conditions and unwanted gradients in properties across the multilayer stack. Although much research is performed so far, a number of interesting issues including the temperature dependence of the magnetic anisotropy (Sugimoto *et al* 1992, Kowalewski *et al* 1993, Barthélemy *et al* 1992), received little attention and still need thorough experimental investigations.

In conclusion, it is found that the experimental determination of PMA, which is intrinsically material and orientation dependent, is sensitive to experimental artefacts such as sample roughness, microstructure (patches and columns), formation of interface alloys and mechanical stresses. Although the influence of several of these factors on the measured anisotropy may be quantified (e.g. roughness, patchiness, mechanical stresses), direct comparison with the predictions from *ab initio* calculations demands caution. Whilst the orientational dependence of the PMA is theoretically confirmed, and encouraging quantitative agreement is established with the measured PMA in several MBE-grown sample series, the major uncertainty associated with the *ab initio* calculations remains the necessity to use a coherent epitaxial structural model, which is infrequently encountered in many important cases: Co/Pd(111), Co/Pt(111). As most of the experimental artefacts result in a reduction of the measured PMA, theoretically predicted values should generally exceed those obtained experimentally. The *ab initio* calculations also predict enhanced orbital moments in several systems which display strong PMA, which have subsequently been confirmed experimentally using MCXD (Weller *et al* 1994). However, enhanced moments are not directly related to large PMA: it is the orbital moment anisotropy which determines the magnitude of the PMA (Weller *et al* 1995). Finally, it was demonstrated that where relaxation from coherent to incoherent epitaxial growth is encountered, the stress apparently contributes to both volume and interface anisotropies, the latter of which may therefore further be separated into a magneto-elastic term (the misfit interface anisotropy) and an electronic term (in fact the result of *ab initio* calculations). Such examples illustrate how recent insights are taking us beyond the phenomenological approach to perpendicular anisotropy.

Acknowledgments

The authors gratefully acknowledge the proof reading of the manuscript by P J van der Zaag and R Jungblut.

References

Albrecht M, Furubayashi T, Przybylski M, Korecki J and Gradmann U 1992 *J. Magn. Magn. Mater.* **113** 207–20

Araki S, Takahata T, Dohnomae H, Okuyama T and Shinjo T 1989 *Proc. Materials Research Society Conf. (Materials Research Society 151)* pp 123–9

Artman J O 1985 *IEEE Trans. Magn.* **21** 1271–3

Awano H, Taniguchi O, Katayama T, Inoue F, Itoh A and Kawanishi K 1988 *J. Appl. Phys.* **64** 6107–9

Bales G S and Zangwill A 1991 *J. Vac. Sci. Technol.* A **9** 145–9

Barthélemy A, Fert A, Etienne P, Cabanel R and Lequien S 1992 *J. Magn. Magn. Mater.* **104–107** 1816–18

Beauvillain P, Bounouh A, Chappert C, Mégy R, Ould-Mahfoud S, Renard J P, Veillet P, Weller D and Corno J 1994 *J. Appl. Phys.* **76** 6078–80

Bennett L H, Swartzendruber L J, Lashmore D S, Oberle R, Atzmony U, Dariel M P and Watson R E 1989 *Phys. Rev.* B **40** 4633–7

Berger A, Linke U and Oepen H P 1992 *Phys. Rev. Lett.* **68** 839–42

Bergholz R and Gradmann U 1984 *J. Magn. Magn. Mater.* **45** 389–98

Bergter E, Gradmann U and Bergholz R 1985 *Solid State Commun.* **53** 565–7

Bian X, Hardner H T and Parkin S S P 1996 *J. Appl. Phys.* **79** 4980–2

Bloemen P J H 1993 *PhD Thesis* Eindhoven University of Technology, The Netherlands

——unpublished

Bloemen P J H and de Jonge W J M 1992 *J. Magn. Magn. Mater.* **116** L1–6

Bloemen P J H, de Jonge W J M and den Broeder F J A 1991 *J. Magn. Magn. Mater.* **93** 105–8

Bloemen P J H, van Alphen E A M, de Jonge W J M and den Broeder F J A 1992a *Proc. Materials Research Society Conf. (Materials Research Society 231)* pp 479–83

Bloemen P J H, den Broeder F J A and de Jonge W J M 1992b *J. Appl. Phys.* **72** 4840–4

Bruno P 1988a *J. Appl. Phys.* **64** 3153–6

——1988b *J. Phys. F: Met. Phys.* **18** 1291–8

——1989 *Phys. Rev.* B **39** 865–8

Bruno P and Renard J-P 1989 *Appl. Phys.* A **49** 499–506

Burd J, Huq M and Lee E W 1977 *J. Magn. Magn. Mater.* **5** 135–41

Cabanel R, Etienne P, Lequien S, Creuzet G, Barthélémy A and Fert A 1990 *J. Appl. Phys.* **67** 5409–11

Carcia P F 1988 *J. Appl. Phys.* **63** 5066–73

Carcia P F, Li Z G and Zeper W B 1993 *J. Magn. Magn. Mater.* **121** 452–60

Carcia P F, Meinhaldt A D and Suna A 1985 *Appl. Phys. Lett.* **47** 178–80

Chang C-A 1990 *J. Appl. Phys.* **68** 4873–5

Chappert C and Bruno P 1988 *J. Appl. Phys.* **64** 5736–41

Chen J and Erskine J L 1992 *Phys. Rev. Lett.* **68** 1212–15

Cherief N, Givord D, Liénard A, Mackay K, McGrath O F K, Rebouillat J P, Robaut F and Souche Y 1993 *J. Magn. Magn. Mater.* **121** 94–101

Childress J R, Chien C L and Jankowski A F 1992 *Phys. Rev.* B **45** 2855–62

Chuang D S, Ballentine C A and O'Handley R C 1994 *Phys. Rev.* B **49** 15 084–95

Chubing P, Daosheng D and Yongbing H 1992 *J. Magn. Magn. Mater.* **110** 113–18

Cochran J F 1994 *Ultrathin Magnetic Structures* vol II, ed B Heinrich and J A C Bland (Berlin: Springer) ch 3.2, pp 222–57

Cochran J F, Heinrich B, Arrott A S, Urquhart K B, Dutcher J R and Purcell S T 1988 *J. Physique* **49** 1671–6

Daalderop G H O 1991b *PhD Thesis* Delft University of Technology, The Netherlands

Daalderop G H O, Kelly P J and den Broeder F J A 1992 *Phys. Rev. Lett.* **68** 682–5

Daalderop G H O, Kelly P J and Schuurmans M F H 1990a *Phys. Rev.* B **41** 11 919–37

——1990b *Phys. Rev.* B **42** 7270–3

——1991a *Phys. Rev.* B **44** 12 054–7

——1994 *Phys. Rev.* B **50** 9989–10 003

de Gronckel H A M, Mertens B M, Bloemen P J H, Kopinga K, and de Jonge W J M 1992 *J. Magn. Magn. Mater.* **104–107** 1809–10

de Jonge W J M, Bloemen P J H and den Broeder F J A 1994 *Ultrathin Magnetic Structures* vol I, ed B Heinrich and J A C Bland (Berlin: Springer) ch 2.3, pp 65–90

de Miguel J J, Cebollada A, Gallego J M, Miranda R, Schneider C M, Schuster P and Kirschner J 1991 *J. Magn. Magn. Mater.* **93** 1–9

den Broeder F J A, Hoving W and Bloemen P J H 1991 *J. Magn. Magn. Mater.* **93** 562–70

den Broeder F J A, Janssen E, Hoving W and Zeper W B 1992 *IEEE Trans. Magn.* **28** 2760–5

den Broeder F J A, Kuiper D, Donkersloot H C and Hoving W 1989 *Appl. Phys.* A **49** 507–12
den Broeder F J A, Kuiper D, van de Mosselaar A P and Hoving W 1988 *Phys. Rev. Lett.* **60** 2769–72
Deubner W 1930 *Ann. Phys., Lpz.* **5** 261–80
de Veirman A E M, Hakkens F J G, Coene W and den Broeder F J A 1992 *Proc. Materials Research Society Conf. (Materials Research Society 263)* pp 119–24
Dinia A, Ounadjela K, Arbaoui A, Suran G, Muller D and Panissod P 1992 *J. Magn. Magn. Mater.* **104–107** 1871–2
Draaisma H J G and de Jonge W J M 1988 *J. Appl. Phys.* **64** 3610–13
Draaisma H J G, den Broeder F J A and de Jonge W J M 1987 *J. Magn. Magn. Mater.* **66** 351–5
Elmers H J and Gradmann U 1990 *Appl. Phys.* A **51** 255–63
Engel B N, England C D, van Leeuwen R A, Wiedmann M H and Falco C M 1991a *Phys. Rev. Lett.* **67** 1910–13
——1991b *J. Appl. Phys.* **70** 5873–5
Engel B N, Wiedmann M H, van Leeuwen R A and Falco C M 1993a *Phys. Rev.* B **48** 9894–7
——1993b *J. Appl. Phys.* **73** 6192–4
——1993c *J. Magn. Magn. Mater.* **126** 532–4
England C D, Bennet W R and Falco C M 1988 *J. Appl. Phys.* **64** 5757–9
Falicov L M *et al* 1990 *J. Mater. Res.* **5** 1299–340
Fassbender J, Mathieu Ch, Hillebrands B, Güntherodt G, Jungblut R and Johnson M T 1995 *J. Magn. Magn. Mater.* **148** 156–7
Feldman L C and Mayer J W 1986 *Fundamentals of Surface and Thin Films Analysis* (Englewood Cliffs, NJ: Prentice-Hall)
Fert A and Bruno P 1994 *Ultrathin Magnetic Structures* vol II, ed B Heinrich and J A C Bland (Berlin: Springer) ch 2.2, pp 82–117
Flanders P J 1988 *J. Appl. Phys.* **63** 3940–5
Freiser M J 1968 *IEEE Trans. Magn.* **4** 152–61
Fritzsche H, Elmers H J and Gradmann U 1994 *J. Magn. Magn. Mater.* **135** 343–54
Fritzsche H, Kohlhepp and Gradmann U 1995 *Phys. Rev.* B **51** 15 933–41
Gay J G and Richter R 1987a *Phys. Rev. Lett.* **56** 2728–31
——1987b *J. Appl. Phys.* **61** 3362–5
Goldman L M, Blanpain B and Spaepen F 1986 *J. Appl. Phys.* **60** 1374–6
Gradmann U 1966 *Ann. Phys., Lpz.* **17** 91–106
Gradmann U, Bergholtz R and Bergter E 1984 *IEEE Trans. Magn.* **20** 1840–5
Gradmann U and Müller J 1968 *Phys. Status Solidi* **27** 313–24
Grolier V, Ferré J, Maiziewski A, Stefanowicz E and Renard D 1993 *J. Appl. Phys.* **73** 5939–41
Gyorgy E M, McWhan D B, Dillon J F Jr, Rupp L W, Testadi L R and Flanders P J 1980 *Phys. Rev. Lett.* **45** 57–60
Hakkens F J G, Coene W and den Broeder F J A 1992 *Proc. Materials Research Society Conf. (Materials Research Society 231)* pp 397–404
Hakkens F J G, de Veirman A E M, Coene W and den Broeder F J A 1993 *J. Mater. Res.* **8** 1019–27
Harp G R and Parkin S S P 1994 *Appl. Phys. Lett.* **65** 3063–5
——unpublished
Hartmann D, Weber W, Wesner D A, Popovic S and Güntherodt G 1993 *J. Magn. Magn. Mater.* **121** 160–2
Harzer J V, Hillebrands B, Stamps R L, Güntherodt G, Weller D, Lee Ch, Farrow R F C and Marinero E E 1992 *J. Magn. Magn. Mater.* **104–107** 1863–4
Hashimoto S, Ochiai Y and Aso K 1989 *J. Appl. Phys.* **66** 4909–16
Heinrich B 1994 *Ultrathin Magnetic Structures* vol II, ed B Heinrich and J A C Bland (Berlin: Springer) ch 3.1, pp 195–222
Heinrich B, Celinski Z, Cochran J F, Arrott A S and Myrtle K 1991a *J. Appl. Phys.* **70** 5769–74
Heinrich B, Cochran J F, Kowalewski M, Kirschner J, Celinski Z, Arrott A S and Myrtle K 1991b *Phys. Rev.* B **44** 9348–61
Heinrich B and Cochran J F 1993 *Adv. Phys.* **42** 523–639
Henry Y, Mény C, Dinia A and Panissod P 1993 *Phys. Rev.* B **47** 15 037–45
Hillebrands B, Boufelfel A, Falco C M, Baumgart P, Güntherodt G, Zirngiebl E and Thompson J D 1988 *J. Appl. Phys.* **63** 3880–4
Hillebrands B, Fassbender J, Jungblut R, Güntherodt G, Roberts D J and Gehring G A 1996 *Phys. Rev.* B **53** 10 548–51
Hillebrands B and Güntherodt G 1994 *Ultrathin Magnetic Structures* vol II, ed B Heinrich and J A C Bland (Berlin: Springer) ch 3.3, pp 258–79

Hillebrands B, Krams P, Fassbender J, Mathieu C, Güntherodt G, Jungblut R and Johnson M T 1994 *Acta Physica Polonica* A **85** 179–93
Hunt R P 1967 *J. Appl. Phys.* **38** 1652–71
Hurdequint H 1991 *J. Magn. Magn. Mater.* **93** 336–40
Johnson M T, de Vries J J, McGee N W E, aan de Stegge J and den Broeder F J A 1992 *Phys. Rev. Lett.* **69** 3575–8
Jungblut R, Johnson M T, aan de Stegge J, Reinders A and den Broeder F J A 1994 *J. Appl. Phys.* **75** 6424–6
Kerr J 1877 *Phil. Mag.* **3** 339–43
Kingetsu T and Sakai K 1993 *J. Appl. Phys.* **73** 7622–6
Kohlhepp J, Elmers H J and Gradmann U 1992 *J. Magn. Magn. Mater.* **121** 487–9
Kohlhepp J and Gradmann U 1995 *J. Magn. Magn. Mater.* **139** 347–54
Kohlhepp J and Jungblut R unpublished
Kohlhepp J, Jungblut R, Hillebrands B and Johnson M T unpublished
Kools J C S 1992 *PhD Thesis* Eindhoven University of Technology, The Netherlands
Kools J C S, Coehoorn R, Hakkens F J G and Fastenau R H J 1993 *J. Magn. Magn. Mater.* **121** 83–7
Kooy C and Enz U 1960 *Philips Res. Rep.* **15** 7–29
Kowalewski M, Schneider C M and Heinrich B 1993 *Phys. Rev.* B **47** 8748–53
Krams P, Lauks F, Stamps R L, Hillebrands B and Güntherodt G 1992 *Phys. Rev. Lett.* **69** 3674–7
Krams P, Lauks F, Stamps R L, Hillebrands B, Güntherodt G and Oepen H P 1993 *J. Magn. Magn. Mater.* **121** 483–6
Krishnan R, Porte M and Tessier M 1992 *J. Magn. Magn. Mater.* **103** 47–9
Kyuno K, Yamamoto R and Asano S 1992 *J. Phys. Soc. Japan* **61** 2099–103
Lamelas F J, Lee C H, Le H, Vavra W and Clarke R 1989 *Proc. Materials Research Society Conf. (Materials Research Society 151)* pp 283–8
Landolt-Börnstein 1986 *Series III* vol 19a (Berlin: Springer) p 43
Le Dang K, Veillet P, Chappert C, Farrow R F C, Marks R F, Weller D and Cebollada A 1994 *Phys. Rev.* B **50** 200–4
Lee C H, He H, Lamelas F J, Vavra W, Uher C and Clarke R 1990 *Phys. Rev.* B **42** 1066–9
Lin C-J, Gorman G L, Lee C H, Farrow R F C, Marinero E E, Do H V, Notarys H and Chien C J 1991 *J. Magn. Magn. Mater.* **93** 194–206
Lugert G, Robl W, Pfau L, Brockmann M and Bayreuther G 1993 *J. Magn. Magn. Mater.* **121** 498–502
Luykx M P M, Swüste C H W, Draaisma H J G and de Jonge W J M 1988 *J. Physique* **49** 1769–70
MacLaren J M and Victora R H 1994 *J. Appl. Phys.* **76** 6069–74
Maksymowicz L J and Jankowski H 1995 *J. Magn. Magn. Mater.* **147** 409–16
Mansuripur M 1990 *J. Appl. Phys.* **67** 6466–75
Matthews J W 1990 *Dislocations in Solids* vol 2, ed F R N Nabarro (Amsterdam: North-Holland) pp 461–545
Matthews J W and Blakeslee A E 1974 *J. Cryst. Growth* **27** 118–25
——1975 *J. Cryst. Growth* **29** 273–80
Matthews J W and Crawford J L 1970 *Thin Solid Films* **5** 187–98
McGee N W E, Johnson M T, de Vries J J and aan de Stegge J 1993 *J. Appl. Phys.* **73** 3418–25
McMichael R D, Atzmony U, Beauchamp C, Bennett L H, Swartzendruber L J, Lashmore D S and Romankiw L T 1992 *J. Magn. Magn. Mater.* **113** 149–54
Mitsuzuka T, Kamijo A and Igarashi H 1990 *J. Appl. Phys.* **68** 1787–90
Nakamura K, Tsunashima S, Hasegawa M and Uchiyama S 1991 *J. Magn. Magn. Mater.* **93** 462–4
Néel L 1954 *J. Physique Rad.* **15** 225–39
Obi Y, Kawano Y, Tange Y and Fujimori H 1991 *J. Magn. Magn. Mater.* **93** 587–91
Oepen H P, Berger A, Schneider C M, Reul T and Kirschner J 1993 *J. Magn. Magn. Mater.* **121** 490–3
Ortega J E, Himpsel F J, Mankey G J and Willis R F 1993 *Phys. Rev.* B **47** 1540–52
Ould-Mahfoud S *et al* 1993 *Proc. Materials Research Society Conf. (Materials Research Society 313)* pp 251–6
Pechan M, Fullerton E E, Robertson W, Grimsditch M and Schuller I K 1995 *Phys. Rev.* B **52** 3045–8
Pechan M and Schuller I K 1987 *Phys. Rev. Lett.* **59** 132–5
Purcell S T, Johnson M T, McGee N W E, de Vries J J, Zeper W B and Hoving W 1993 *J. Appl. Phys.* **73** 1360–7
Purcell S T, Johnson M T, McGee N W E, Zeper W B and Hoving W 1992 *J. Magn. Magn. Mater.* **113** 257–63
Purcell S T, van Kesteren H W, Cosman E C and Hoving W 1991 *J. Magn. Magn. Mater.* **93** 25–30
Robl W and Bayreuther 1993 *EPS Conf. (Regensburg)*
Sakurai M 1994 *Phys. Rev.* B **50** 3761–6
Sakurai M, Takahata T and Moritani I 1991 *J. Magn. Soc. Japan.* **15** 411–14
Sato K 1981 *Japan. J. Appl. Phys.* **20** 2403–9

Schäfer R, Hubert A and Parkin S S P 1993 *IEEE Trans. Magn.* **29** 2738–40
Schulz B and Baberschke K 1994 *Phys. Rev.* B **50** 13 467–71
Schulz B, Schwarzwald R and Baberschke K 1994 *Surf. Sci.* **307** 1102–8
Smardz L, Szymański B, Barnaś J and Baszyński J 1992 *J. Magn. Magn. Mater.* **104–107** 1885–6
Smithells C J 1976 *Metals Reference Book* (New York: Butterworths) p 978
Sugimoto T, Katayama T, Suzuki Y, Hashimoto M, Nishihara Y, Itoh A and Kawanishi K 1992 *J. Magn. Magn. Mater.* **104–107** 1845–6
Suits J C 1972 *IEEE Trans. Magn.* **8** 95–105
Swaving S, Gerritsma G J, Lodder J C and Popma Th J A 1987 *J. Magn. Magn. Mater.* **67** 155–64
Takahata T, Araki S and Shinjo T 1989 *J. Magn. Magn. Mater.* **82** 287–93
Tokunaga T, Kohri M, Kadomatsu H and Fujiwara H 1981 *J. Phys. Soc. Japan* **50** 1411–12
Toney M F, Farrow R F C, Marks R F, Harp G R and Rabadeau T A 1992 *Proc. Materials Research Society Conf. (Materials Research Society 263)* pp 237–42
Újfalussy B, Szunyogh L, Bruno P and Weinberger P 1996 *Phys. Rev. Lett.* **77** 1805–8
van Alphen E A M, de Gronckel H A M, Bloemen P J H, van Steenbergen A S and de Jonge W J M 1993 *J. Magn. Magn. Mater.* **121** 77–9
van Alphen E A M, te Veldhuis S G E, de Gronckel H A M, Kopinga K and de Jonge W J M 1994 *Phys. Rev.* B **49** 17 336–41
van der Merwe J H 1963 *J. Appl. Phys.* **34** 123–7
van Leeuwen R A, England C D, Dutcher J R, Falco C M, Bennet W R and Hillebrands B 1990 *J. Appl. Phys.* **67** 4910–12
van Vleck J H 1937 *Phys. Rev.* **52** 1178–98
Victora R H and MacLaren J M 1993a *J. Appl. Phys.* **73** 6415–17
——1993b *Phys. Rev.* B **47** 11 583–6
Weber W, Back C H, Ramsperger U, Vaterlaus A and Allenspach R 1995 *Phys. Rev.* B **52** R14 400–3
Weller D, Farrow R F C, Marks R F, Harp G R, Notarys H and Gorman G 1993 *Proc. Materials Research Society Conf. (Materials Research Society 313)* pp 791–7
Weller D, Stöhr J, Carl A, Samant M G, Chappert C, Mégy R, Beauvillain P, Veillet P and Held G A 1995 *Phys. Rev. Lett.* **75** 3752–5
Weller D, Wu Y, Stöhr J, Samant M G, Hermsmeier B D and Chappert C 1994 *Phys. Rev.* B **49** 12 888–96
Wiedmann M H, Engel B N, van Leeuwen R A, Mibu K, Shinjo T and Falco C M 1993 *Metal. Artificial Superlatt.* **313** 531–6
Xiao G and Chien C L 1987 *J. Appl. Phys.* **61** 4061–3
Zeper W B 1991 *PhD Thesis* Technical University Twente, The Netherlands
Zeper W B and Carcia P F 1989 *IEEE Trans. Magn.* **25** 3764–6
Zijlstra H 1967 *Experimental Methods in Magnetizm* vol II, ed E P Wohlfarth (Amsterdam: North-Holland)